



Lead isotopes in deep-sea coral skeletons: Ground-truthing and a first deglacial Southern Ocean record

David J. Wilson^{a,*}, Tina van de Flierdt^a, Jess F. Adkins^b

^a Department of Earth Science and Engineering, Imperial College London, London SW7 2AZ, United Kingdom

^b Caltech Division of Geology and Planetary Sciences, MS 131-24, Caltech, Pasadena, CA 91125, USA

Received 21 August 2016; accepted in revised form 31 January 2017; available online 9 February 2017

Abstract

Past changes in seawater lead (Pb) isotopes record the temporal evolution of anthropogenic pollution, continental weathering inputs, and ocean current transport. To advance our ability to reconstruct this signature, we present methodological developments that allow us to make precise and accurate Pb isotope measurements on deep-sea coral aragonite, and apply our approach to generate the first Pb isotope record for the glacial to deglacial mid-depth Southern Ocean.

Our refined methodology includes a two-step anion exchange chemistry procedure and measurement using a ^{207}Pb – ^{204}Pb double spike on a Thermo Finnigan Triton TIMS instrument. By employing a $10^{12}\ \Omega$ resistor (in place of a $10^{11}\ \Omega$ resistor) to measure the low-abundance ^{204}Pb ion beam, we improve the internal precision on $^{206,207,208}\text{Pb}/^{204}\text{Pb}$ for a 2 ng load of NIST-SRM-981 Pb from typically ~ 420 ppm to ~ 230 ppm (2 s.e.), and the long term external reproducibility from ~ 950 ppm to ~ 550 ppm (2 s.d.). Furthermore, for a typical 500 mg coral sample with low Pb concentrations (~ 6 – 10 ppb yielding ~ 3 – 5 ng Pb for analysis), we obtain a comparable internal precision of ~ 150 – 250 ppm for $^{206,207,208}\text{Pb}/^{204}\text{Pb}$, indicating a good sensitivity for tracing natural Pb sources to the oceans. Successful extraction of a seawater signal from deep-sea coral aragonite further relies on careful physical and chemical cleaning steps, which are necessary to remove anthropogenic Pb contaminants and obtain results that are consistent with ferromanganese crusts.

Applying our approach to a collection of late glacial and deglacial corals (~ 12 – 40 ka BP) from south of Tasmania at ~ 1.4 – 1.7 km water depth, we generated the first intermediate water Pb isotope record from the Southern Ocean. That record reveals millennial timescale variability, controlled by binary mixing between two Pb sources, but no distinct glacial-interglacial Pb isotope shift. Mixing between natural endmembers is fully consistent with our data and points to a persistence of the same Pb sources through time, although we cannot rule out a minor influence from recent anthropogenic Pb. Whereas neodymium (Nd) isotopes in the Southern Ocean respond to global ocean circulation changes between glacial and interglacial periods, Pb isotopes record more localised mixing within the Antarctic Circumpolar Current, potentially further modulated by climate through changing terrestrial inputs from southern Africa or Australia. Such decoupling between Pb and Nd isotopes in the Southern Ocean highlights their potential to provide complementary insights into past oceanographic variability.

Keywords: Southern Ocean; Tasmania; Deglaciation; Climate change; Ocean circulation; Weathering; Isotope tracers; Pb isotopes; Deep-sea corals

© 2017 The Author(s). Published by Elsevier Ltd. This is an open access article under the CC BY license (<http://creativecommons.org/licenses/by/4.0/>).

Keywords: Southern Ocean; Tasmania; Deglaciation; Climate change; Ocean circulation; Weathering; Isotope tracers; Pb isotopes; Deep-sea corals

* Corresponding author.

E-mail address: david.wilson1@imperial.ac.uk (D.J. Wilson).

1. INTRODUCTION

1.1. Motivation

The oceanic distribution of radiogenic isotope tracers, such as neodymium (Nd), lead (Pb) and hafnium (Hf), provides valuable evidence on continental weathering sources and ocean circulation in the present and past oceans (see reviews by Frank, 2002; Goldstein and Hemming, 2003). Given differences between these elements in their continental weathering behaviour and/or oceanic residence times, there is significant potential for a multi-isotope approach to provide better constraints on those processes. Indeed, studies on ferromanganese crusts have explored such scenarios on million-year timescales, including the Neogene decoupling between Nd and Pb isotopes in the Indian Ocean linked to evolving Himalayan Pb inputs (Frank and O'Nions, 1998), and the decoupling of Nd and Hf isotopes in the North Atlantic attributed to changing erosional and weathering regimes (Piotrowski et al., 2000; van de Flierdt et al., 2002). However, while ferromanganese crusts represent a valuable archive of past seawater compositions, typical sampling approaches integrate over 10^4 – 10^6 years of crust growth. Considering the short oceanic residence times of these elements and the timescales of ocean mixing, higher resolution reconstructions at hundred-year to thousand-year timescales would be valuable for resolving glacial-interglacial to sub-millennial changes and fully exploiting such a multi-isotope approach.

Neodymium isotopes have become relatively well established as a tracer in Quaternary paleoceanography and may now be reconstructed at sub-millennial resolution from fish teeth and foraminifera in sediment cores (Roberts et al., 2010; Tachikawa et al., 2014), and potentially at centennial resolution from deep-sea corals (Colin et al., 2010; van de Flierdt et al., 2010; Wilson et al., 2014). In contrast, Pb isotopes have received less attention – to date no records have been published from foraminifera, while fish teeth appear to be an unsuitable archive for Pb isotopes (Basak et al., 2011). Records of Pb isotope changes over shorter time periods have therefore been based on micro-drilling or laser-ablation of ferromanganese crusts (e.g. Abouchami et al., 1997; Claude-Ivanaj et al., 2001; Foster and Vance, 2006), or acid-reductive leaching in marine sediment cores (e.g. Gutjahr et al., 2009; Crocket et al., 2012; Wilson et al., 2015a), with the majority of these studies carried out in the North Atlantic region to assess changes in weathering mechanisms or fluxes in response to glaciation. However, the above approaches cannot be universally applied in all settings and will often provide only modest time resolution. In particular, while the Southern Ocean is an important region for water mass ventilation and mixing, and one in which ferromanganese crusts and nodules document spatially variable Pb isotopes (Abouchami and Goldstein, 1995), it is a challenging setting for sediment-based approaches and at present there are no glacial-interglacial Pb isotope records from this region.

Given the success of Nd isotope reconstructions from deep-sea corals, our aim here is to explore the suitability of deep-sea coral aragonite for reconstructing Pb isotopic

compositions of the pre-anthropogenic oceans, and to provide a first paleoceanographic case study from the deglacial Southern Ocean near Tasmania. Building upon previous studies tracing anthropogenic Pb using Pb isotopes in surface corals (e.g. Shen and Boyle, 1987; Kelly et al., 2009; Lee et al., 2014), and most recently in deep-sea corals (Lee et al., 2017), our study represents the first coral-based attempt to resolve temporal variability in Pb isotopes in the pre-anthropogenic oceans.

1.2. Lead and Pb isotopes in the oceans

Lead has four naturally-occurring isotopes, with the radiogenic isotopes ^{206}Pb , ^{207}Pb and ^{208}Pb produced from the decay series of ^{238}U , ^{235}U and ^{232}Th , respectively, while ^{204}Pb is non-radiogenic and entirely primordial. These multiple semi-independent isotopes reflect time-integrated U/Pb and Th/Pb ratios of their sources, making Pb isotopes a powerful source tracer, both for sediment provenance and for dissolved inputs to the oceans. With a short deep ocean residence time of ~ 50 – 200 years (Cochran et al., 1990; Henderson and Maier-Reimer, 2002), the dissolved Pb isotopic distribution is controlled by both continental inputs (e.g. weathering and dust) and water mass mixing at a basin scale (e.g. Abouchami and Goldstein, 1995; see also review by Frank, 2002). In comparison to Nd isotopes, which have a longer deep ocean residence time of ~ 300 – 1000 years (Tachikawa et al., 1999; Siddall et al., 2008; Arsouze et al., 2009), Pb isotopes are expected to be more sensitive to local inputs and regional scale mixing (Abouchami and Goldstein, 1995; von Blanckenburg et al., 1996; Vlastelic et al., 2001). Such differing characteristics may help to explain the greater spatial variability of Pb isotopes than Nd isotopes in Southern Ocean ferromanganese nodules (Abouchami and Goldstein, 1995), pointing to their complementary value as ocean tracers.

Our understanding of Pb isotopes in the oceans has come predominantly from measurements on historical and modern seawater; from early pioneering work (e.g. Schaule and Patterson, 1981; Shen and Boyle, 1988b), through to the inclusion of Pb isotopes as a key parameter in the international GEOTRACES programme (e.g. Boyle et al., 2014; Noble et al., 2015). These studies indicate that the modern oceanic Pb cycle has been dominated by anthropogenic inputs since the industrial revolution. In particular, Pb concentrations and isotopes in the North Atlantic Ocean track the changing anthropogenic Pb inputs through time and their subsequent dispersal by ocean circulation, with Pb carried into the deep ocean by ventilation of the thermocline (Shen and Boyle, 1988b) and by sinking and advection of North Atlantic Deep Water (Alleman et al., 1999). Through time, that tongue of anthropogenic Pb has deepened, likely due to a combination of both mixing and semi-reversible particle scavenging (Sherrell et al., 1992; Noble et al., 2015). Anthropogenic Pb inputs from Europe and North America have decreased dramatically since the 1970s (Kelly et al., 2009) and the Indian and northwest Pacific Oceans are now seeing the most significant anthropogenic inputs (e.g. Echevoyen et al., 2014; Lee et al., 2015). In the South Atlantic region, Pb isotopes

trace ocean transport in the Agulhas Current due to the distinct Pb isotope signatures of modern Indian surface waters (Paul et al., 2015b). It is also clear that no part of the global ocean has remained unperturbed by anthropogenic Pb, including waters around Antarctica (Flegal et al., 1993) and the abyssal depths of the Pacific Ocean (Schaule and Patterson, 1981; Wu et al., 2010), with the latter observation testifying to the role of particles in transporting Pb into the deep ocean even in regions that have not been recently ventilated.

Although such seawater studies guide our understanding of Pb as a tracer, they also highlight a complication for paleoceanographic studies because the modern seawater Pb isotopic composition reflects a strong overprinting of natural source signatures by anthropogenic inputs. In addition, in many locations, the Pb isotopic composition and concentrations are changing rapidly through time (Noble et al., 2015; Lee et al., 2017), providing a further challenge to calibration efforts. Therefore, despite their low resolution for generating paleoceanographic records, ferromanganese crust compositions provide valuable evidence on pre-anthropogenic Pb compositions of seawater.

1.3. Potential of Pb isotopes in deep-sea corals as a pre-anthropogenic ocean tracer

Deep-sea corals have recently emerged as a versatile archive for reconstructing past chemical oceanographic changes (e.g. Robinson et al., 2014). In particular, they are suitable for U–Th dating, providing both absolute ages and the potential for reconstructing changes at approximately centennial resolution during the last deglaciation. That capability has enabled high resolution studies using multiple proxies, including radiocarbon for ocean ventilation (e.g. Chen et al., 2015), clumped isotopes for temperature (e.g. Thiagarajan et al., 2014) and Nd isotopes for water mass sourcing (e.g. Colin et al., 2010; Wilson et al., 2014). Including Pb isotopes in this multi-proxy approach would be valuable, which motivates the exploration of deep-sea corals as a potential archive for seawater Pb isotopic compositions.

Measurements of both Pb concentrations and Pb isotopes have previously been made on annually-banded aragonitic corals from the surface ocean, in particular to extend historical records of anthropogenic Pb pollution beyond the earliest reliable seawater measurements (e.g. Shen and Boyle, 1987; Kelly et al., 2009; Lee et al., 2014). Those studies indicate an apparent distribution coefficient (K_d) for Pb between seawater and aragonite of ~ 2 – 4 (see also Shen and Boyle, 1988a). In addition, there is good agreement between Pb isotope data from corals and seawater measurements where they overlap in time (Kelly et al., 2009), indicating a clear potential of coral aragonite to record seawater Pb isotopic compositions.

Although Pb isotope measurements are well established in surface corals, the deep ocean has lower Pb concentrations than the surface ocean due to the strong sensitivity of Pb to particle scavenging, while the pre-anthropogenic oceans likely had 10–20 times lower Pb concentrations than the modern or recent oceans (Schaule and Patterson, 1981;

Kelly et al., 2009). These factors make it a potentially more challenging task to measure Pb isotopes in fossil deep-sea corals. To date, only one study has presented Pb isotope data from a deep-sea coral, which focused on tracing the incursion of anthropogenic Pb in recent centuries to decades (Lee et al., 2017), while Pb isotopes in corals have not yet been applied to resolve changes in the pre-anthropogenic oceans. Considering the low end of modern deep ocean Pb concentrations from the Indian Ocean (e.g. 1.5–5 pmol/kg; Echegoyen et al., 2014) to approximate the pre-anthropogenic oceans, Pb concentrations in deep-sea coral aragonite are expected to be low i.e., ~ 1 – 4 ppb (Pb/Ca ~ 0.5 – 2 nmol/mol) assuming a K_d of ~ 2 – 4 similar to surface corals (Shen and Boyle, 1988a), or < 20 ppb (Pb/Ca < 10 nmol/mol) based on a K_d of ~ 3 – 20 observed for deep-sea corals (Adkins et al., 2004; Lee et al., 2017). Consequently, there may be a high possibility for diagenetic or anthropogenic Pb contamination, while accurate and precise measurements on only a few nanograms of Pb require low blank levels and high sensitivity mass spectrometry. In addition, whereas measurements of the major isotope ratios (i.e., $^{206}\text{Pb}/^{207}\text{Pb}$ and $^{208}\text{Pb}/^{207}\text{Pb}$) are generally considered sufficient for tracing anthropogenic Pb sources with highly variable isotopic compositions (e.g. Kelly et al., 2009; Lee et al., 2017), we anticipate that measuring the minor isotope ^{204}Pb ($\sim 1.4\%$ of total Pb) would be valuable in order to fully exploit this isotope system for tracing natural sources in the pre-anthropogenic oceans.

1.4. Outline of this study

Here we assess the viability of measuring Pb isotopes in deep-sea coral aragonite, building upon previous studies that measured Nd isotopes in fossil deep-sea corals (van de Flierdt et al., 2010; Crockett et al., 2014) and a recently developed method for high precision seawater Pb isotope measurements by TIMS (Paul et al., 2015a). To this end, we present a further methodological advance for our TIMS methodology, by using a $10^{12} \Omega$ resistor for the ^{204}Pb measurement on sample sizes of ~ 2 ng Pb. We also determine appropriate sample processing and chemical separation techniques for carbonate samples, using an in-house coral standard, the USGS BCR-2 rock standard, and procedural blank tests. We use physical and chemical coral cleaning experiments to assess the requirements for removing detrital or ferromanganese oxide coatings and potential anthropogenic contaminants. Finally, we apply our refined methodology to generate the first late glacial and deglacial Southern Ocean Pb isotope record from intermediate water depths near Tasmania. This new data can be interpreted in terms of past changes in Pb sources and ocean current transport, in relation to regional and global climatic change.

2. METHODS

2.1. Samples and oceanographic setting

Our study is based on a collection of deep-sea scleractinian corals that were collected by the deep submergence vehicle JASON on cruise TN-228 of the *R/V Thompson*

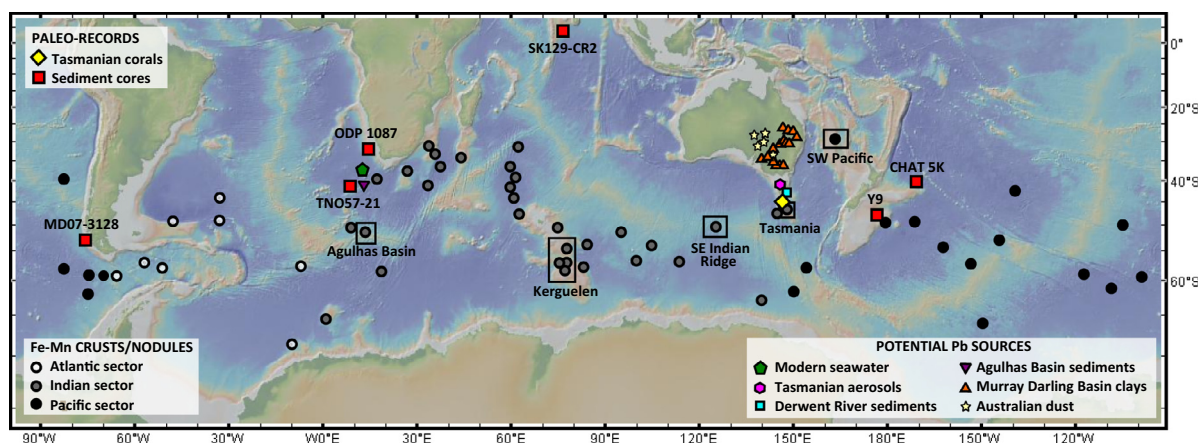


Fig. 1. Location of deep-sea corals south of Tasmania (yellow diamond) in comparison to the locations of other paleoceanographic records (red squares), Southern Ocean ferromanganese crusts and nodules (circles), and potential regional Pb sources (various symbols). Ferromanganese crusts and nodules are from [Abouchami and Goldstein \(1995\)](#) (all samples), [von Blanckenburg et al. \(1996\)](#) (their southern-most three samples) and [Vlastelic et al. \(2001\)](#) (their samples from the Agulhas Basin, Crozet Basin, Kerguelen Plateau, and Australian-Antarctic Basin), and are distinguished by sector as in those studies: Atlantic (70°W to 0), Indian (0 to 148°E), Pacific (148°E to 70°W). Particular samples are highlighted in black boxes: Tasmanian sample SO-36/52KD ([von Blanckenburg et al., 1996](#)); Kerguelen samples DR8604, DR8605, DR8607 and DR8608 ([Vlastelic et al., 2001](#)); Agulhas Basin sample V29-D6 ([Vlastelic et al., 2001](#)); southwest Pacific sample SO-36/63KD ([van de Flierdt et al., 2004a](#)); and Southeast Indian Ridge sample E-PhC/54-6 ([Vlastelic et al., 2001](#)). Anthropogenic Pb sources include modern seawater (South Atlantic; cruise D357, station 3, 36°S, 13°E; [Paul et al., 2015a](#)); Tasmanian aerosols ([Bollhofer and Rosman, 2000](#)); and recent sediments from the Derwent River, Tasmania ([Townsend and Seen, 2012](#)). Natural Pb sources include pre-anthropogenic sediments from the Derwent River, Tasmania ([Townsend and Seen, 2012](#)); detrital sediments from the northern Agulhas Basin (cores ODP 1088–1090; [Noble et al., 2012](#)); clays from the Murray Darling Basin ([de Deckker et al., 2010](#); [de Deckker and Norman, 2010](#)); and chemically extracted fine fractions from Australian dust source areas ([Vallelonga et al., 2010](#)). Paleoceanographic records are from MD07-3128 (1.03 km water depth; [Lamy et al., 2015](#)); TNO57-21 (~5.0 km; [Piotrowski et al., 2008, 2012](#)); ODP 1087 (~1.4 km; [Hu et al., 2016](#)); SK129-CR2 (~3.8 km; [Wilson et al., 2015b](#)); CHAT 5K (~4.2 km; [Noble et al., 2013](#)); and Y9 (~1.3 km; [Hu et al., 2016](#)). Basemap from GeoMapApp. (For interpretation of the references to colour in this figure legend, the reader is referred to the web version of this article.)

south of Tasmania in 2008–2009 ([Thiagarajan et al., 2013](#)). In total, more than 10,000 specimens of *Desmophyllum dianthus* were collected from ~0.8–2.4 km water depths on the Tasmanian Seamounts (43–47°S, 144–152°E) (Fig. 1). Our deglacial Pb isotope record was generated on 25 fossil specimens that were mostly collected from ~1.4–1.7 km water depth (Fig. 2) at the Tasman Shelf setting ([Thiagarajan et al., 2013](#)). The majority of those samples were precisely dated by U–Th isotopes by [Hines et al. \(2015\)](#), while U–Th data from a few additional samples that were not previously published are presented in [Table S1](#). In addition, we present coral cleaning experiments that were carried out on an undated fossil coral specimen that was collected south of Tasmania on cruise SS01-2008 of the *R/V Southern Surveyor* in the location of Sisters Pinnacles (44°S, 147°E, ~1.2 km water depth).

The oceanography in this region (Fig. 2) involves a complex interplay between Upper Circumpolar Deep Water (UCDW) and Pacific Deep Water (PDW) at mid-depths, overlain by Antarctic Intermediate Water (AAIW) above ~1.2 km ([Sokolov and Rintoul, 2000](#); [Macdonald et al., 2009](#); [Bostock et al., 2013](#)) and underlain by Lower Circumpolar Deep Water (LCDW). The sample used for our cleaning experiments was collected from within the deepest levels of the modern AAIW depth range (Fig. 2a), whereas the deglacial record is based on corals collected at depths predominantly influenced by a mixture of UCDW and PDW at present (Fig. 2a,b).

2.2. Physical and chemical cleaning

The aim of physical and chemical cleaning is to remove potential sources of contamination from detrital particles, ferromanganese coatings or anthropogenic contaminants that may be associated with fossil coral skeletons, allowing measurements to be made on the coral aragonite itself. Cleaning procedures for deep-sea corals have previously been assessed for Nd isotopes ([van de Flierdt et al., 2010](#); [Crocket et al., 2014](#)), building upon methods developed for other trace elements ([Shen and Boyle, 1988a](#); [Lomitschka and Mangini, 1999](#); [Cheng et al., 2000](#)). Given the higher Pb/Nd expected in ferromanganese coatings compared to seawater (and therefore coral aragonite), mass balance considerations suggest that cleaning may be even more important for reliable Pb isotope measurements. In addition, the Pb isotope system is sensitive to anthropogenic Pb contaminants, which also need to be removed.

Our cleaning procedure closely followed that of [van de Flierdt et al. \(2010\)](#) and is summarised only briefly here. Physical cleaning involved diamond blade drilling with a Dremel tool to remove potential ferromanganese coatings and detrital sediment from the exterior, while interior cavities or discoloured patches within the skeleton were cut away. The subsequent chemical cleaning procedure included repeated oxidative and reductive steps and is fully described in [Table S2](#). The first cleaning steps (i.e., pre-cleaning) were carried out in a non-classified clean room using acid-cleaned

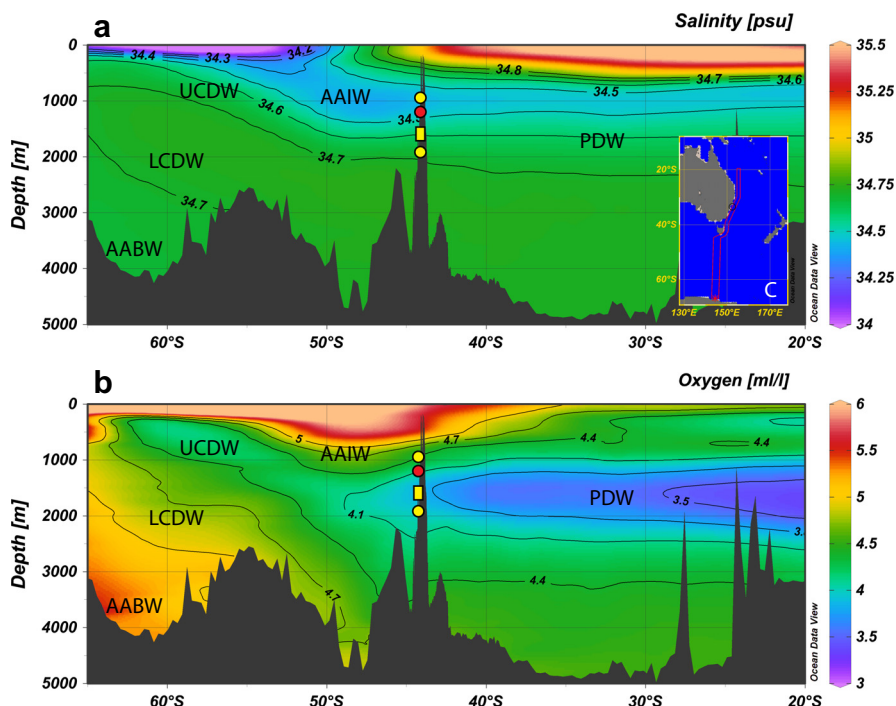


Fig. 2. Oceanographic setting of deep-sea corals collected from south of Tasmania. Plots show (a) salinity section (Zweng et al., 2013), (b) oxygen section (Garcia et al., 2014), and (c) transect line in map view. Coral sample locations are shown schematically with yellow box (majority of deglacial corals), yellow circles (outlying shallower and deeper deglacial corals) and red circle (coral used for cleaning experiments). For detailed sample locations, see Fig. 1b of Thiagarajan et al. (2013). Major water masses are labelled: AABW = Antarctic Bottom Water; AAIW = Antarctic Intermediate Water; LCDW = Lower Circumpolar Deep Water; PDW = Pacific Deep Water; UCDW = Upper Circumpolar Deep Water. Data visualised in Ocean Data View (Schlitzer, 2015). Note that in order to emphasise interior-ocean features, some of the surface and shallow subsurface data extend to values outside the limits of the salinity and oxygen colour scales. (For interpretation of the references to colour in this figure legend, the reader is referred to the web version of this article.)

15 mL Falcon centrifuge tubes, while subsequent cleaning steps used acid-cleaned 15 mL Teflon centrifuge tubes. The final cleaning steps, which used EDTA for the removal of any adsorbed trace metals and dilute nitric acid (0.2%) for surface leaching, were carried out in a Class 10 laminar flow hood within a Class 1000 clean room.

2.2.1. Coral cleaning experiments

We carried out a series of cleaning experiments on six subsampled pieces of the same fossil coral skeleton from cruise SS01-2008 (samples A–F). For each sample, the coral was broken into 30–50 mg pieces before being subjected to chemical cleaning.

(A) Sample A: 1.39 g of physically cleaned coral was split into two equal portions for separate chemical cleaning, before recombining for digestion. The digest was then split into three separate aliquots for column chemistry (A.1, A.2, A.3), of which A.3 was subjected to an additional aqua regia step before column chemistry. Samples A.1 and A.3 were analysed individually for their isotopic compositions by TIMS, while sample A.2 was split into multiple aliquots before TIMS analysis, allowing measurements to be made on both large (~45 ng) and small (~1.5 ng) quantities of Pb.

- (B) Sample B: 0.59 g of physically cleaned coral was chemically cleaned and represents a full replicate of sample A.
- (C) Sample C: 0.47 g of physically cleaned coral was chemically cleaned and also represents a replicate of sample A, but in this case it was crushed to a fine sand in an agate mortar before chemical cleaning.
- (D) Sample D: 0.35 g of coral was chemically cleaned but not physically cleaned beforehand.
- (E) Sample E: 0.36 g of coral was not physically or chemically cleaned, but was subjected to the final three rinses of the cleaning procedure (i.e., nitric acid, EDTA and nitric acid) in order to remove potential surface contaminants.
- (F) Sample F: 0.20 g of coral was physically but not chemically cleaned, and was then subjected to the final three rinses of the cleaning procedure in order to remove potential surface contaminants (as for sample E). Due to sample limitation, this sample was a smaller size and it was taken from near the base of the coral rather than from within the upper septae.

2.3. Laboratories and reagents

All subsequent preparation was carried out in Class 10 laminar flow hoods within the Class 1000 MAGIC clean

room facility at Imperial College London. Milli-Q water from a Millipore system (resistivity >18.2 M Ω) and Savillex Teflon vials were used throughout. The acids used were either Optima/Suprapure grade (concentrated HBr) or were distilled in-house from reagent grade acids in quartz stills or Savillex Teflon stills (~16 M HNO₃ and ~6 M HCl). Lead blanks for these acids were typically <2 pg/mL. Teflon vials were cleaned in both 6 M HCl and 2 M HNO₃ on hotplates at ~100 °C, before being individually refluxed twice in 2 M HNO₃. Teflon columns were also cleaned in heated 3 M HCl, 2 M HNO₃ and dilute HNO₃ between use, which was important to avoid Pb retention contributing to procedural Pb blanks.

2.4. Sample and standard preparation

Following cleaning, coral samples were digested in 6 M HCl (around 10% in excess of that required to digest the carbonate). The sample solution was dried down and converted multiple times to bromide form, before dissolution in 5 mL or 10 mL 2 M HBr in preparation for column chemistry.

An in-house coral Pb standard was prepared from the same coral powder that was used for the coral Nd standard in [Crocket et al. \(2014\)](#). Approximately 129.11 g of coral powder was dissolved in 500 mL of ~6 M HCl. It was centrifuged to allow remaining solid material to be removed and subsequently stored as a stock solution in a large Teflon beaker. An aliquot was spiked with our ²⁰⁷Pb–²⁰⁴Pb double spike, put through column chemistry and its isotopic composition measured, allowing us to determine its Pb concentration as ~77 ng/mL, reflecting approximate Pb concentrations in the coral powder of ~310 ppb (Pb/Ca ~150 nmol/mol). This concentration is much higher than typical Pb concentrations in cleaned corals (see later), which may reflect the less rigorous cleaning applied to the standard material (i.e., only sand-blasting, with no use of the Dremel tool for careful physical cleaning, and no chemical cleaning or rinsing). A similar observation was described for Nd by [Crocket et al. \(2014\)](#).

A BCR-2 rock standard was prepared by digesting 87.58 mg of BCR-2 powder in a mixture of 2.5 mL concentrated HF and 0.625 mL concentrated HNO₃. It was refluxed on a hotplate at 140 °C for 3 days, dried down, and converted to HNO₃ three times. It was then dried down and taken up in 9.652 mL ~6 M HCl and refluxed on a hotplate at 120 °C overnight, to give a stock BCR-2 solution with an expected Pb concentration of 100 ng/mL.

2.5. Column chemistry for elemental separation

Elemental separation of the Pb from the carbonate matrix was based on a two-step HBr–HNO₃ anion exchange chemistry using AG1-X8 resin, adapted from [Paul et al. \(2015a\)](#) after [Lugmair and Galer \(1992\)](#). Two column steps were employed in order to remove matrix elements (e.g. calcium) sufficiently well to achieve good ionisation of Pb for analysis by TIMS. Our first column step followed that employed by [Paul et al. \(2015a\)](#), except for omitting trace HF from the HBr solutions, which had been introduced

in that study to prevent re-precipitation of Si from the seawater sample matrix after co-precipitation. In brief, we used 100 μ L shrink-fit Teflon columns with an internal diameter of ~3 mm and a reservoir volume of ~2 mL that were filled with AG1-X8 100–200 mesh resin. After equilibration with 2 \times 0.1 mL 2 M HBr, samples were loaded in 5 mL 2 M HBr, the matrix was eluted in 2 \times 0.1 mL 2 M HBr, 2 \times 0.5 mL 0.2 M HBr–0.5 M HNO₃, and 0.2 mL 0.03 M HBr–0.5 M HNO₃, and finally the Pb fraction was eluted in 3 mL 0.03 M HBr–0.5 M HNO₃.

For the second (clean-up) step, we initially followed the second column step of [Paul et al. \(2015a\)](#) scaled for 100 μ L columns. However, we observed a significant loss of Pb during that second step, for both the NIST-SRM-981 Pb standard and our in-house coral standard, leading to yields of ~60–70%, consistent with the column yields reported by [Paul et al. \(2015a\)](#). This loss of Pb was overcome by instead repeating the first column step a second time. In that case, based on tests on our in-house coral standard, two passes through 100 μ L columns lead to a good yield (better than 90%) when processing the equivalent of ~200 mg of coral, while the yield declines rapidly above ~300 mg ([Fig. 3](#)), indicating saturation of the resin by matrix elements. Therefore, for our target coral sample size of ~400–500 mg, the dissolved samples were split into two aliquots for the first column step, before being re-combined for the second (clean-up) column step. A more elegant approach for future studies might instead use larger 200 μ L columns for the first step and modify the acid volumes accordingly.

Chemistry batches included in-house coral standards (large: 400 μ L, ~31 ng Pb; small: 40 μ L, ~3.1 ng Pb), BCR-2 rock standards (typically 20 μ L, ~2 ng Pb) and blanks. Measured blanks included column blanks,

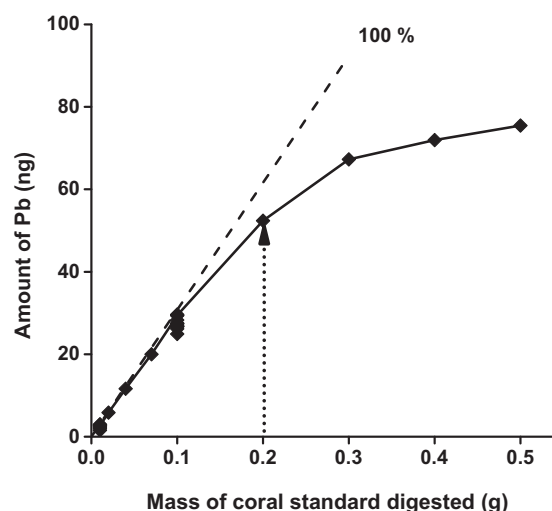


Fig. 3. Column yields for our in-house coral standard based on two-stage ion exchange chemistry using 100 μ L columns, as described in the text. The symbols and solid line show the observed yields, whereas the dashed line indicates the expected relationship for a 100% column yield. Note that yields are better than ~90% for up to 0.2 g of coral (vertical dotted arrow), beyond which yields diminish significantly.

combined digestion and column blanks, and full procedural blanks, all of which were treated identically to samples from the appropriate stages of the process.

2.6. Lead isotope measurements by TIMS using a ^{207}Pb – ^{204}Pb double spike

Lead isotope measurements were made using a ^{207}Pb – ^{204}Pb double spike on a Thermo Finnigan Triton TIMS, building on the seawater method pioneered by Paul et al. (2015a). The approach to analyse both unspiked and spiked samples is the most precise and accurate way to correct for instrumental mass fractionation in a system without an invariant non-radiogenic isotope pair (e.g. Hamelin et al., 1985; Galer, 1999; Thirlwall, 2000; Taylor et al., 2015). After column chemistry, a small aliquot (typically $\sim 10\%$) was analysed in order to establish approximate Pb concentrations on a NuPlasma MC-ICP-MS and thereby determine optimal spiking. The remaining sample was split, with 2/3 used for the unspiked measurement and 1/3 used for the spiked measurement. The double spike prepared by Paul et al. (2015a) had a composition of $^{207}\text{Pb}/^{204}\text{Pb} = 1.03181$ and the target spike/sample ratio was ~ 1.2 (Rudge et al., 2009). The unspiked and spiked Pb solutions were fully evaporated, re-dissolved in 1.5 μL 2 M HNO_3 , loaded on previously degassed zone-refined Re (99.999%, H Cross, USA) single filaments, and dried at 0.4 A. Approximately 0.4 μL of silica-gel activator (made from silica nanoparticles in 0.16 M phosphoric acid) was added and dried at 0.4 A, before final heating up to 1.8–2.0 A to evaporate the phosphoric acid and fuse the gel. After loading the sample turret into the TIMS source, the source was baked for 3 h and allowed to cool for at least 8 h before starting measurements. As described in Paul et al. (2015a) (and references therein), source baking has multiple benefits of reducing the source pressure, fusing the silica gel, improving beam stability, and reducing potential hydrocarbon interferences.

Lead isotope measurements were made in static mode using Faraday cups fitted with $10^{11} \Omega$ resistors, except for the simultaneous measurement of the ^{204}Pb ion beam, for which we tested and proceeded to use a $10^{12} \Omega$ resistor to improve precision on the ratios including this minor isotope. Due to the longer decay time of $10^{12} \Omega$ than $10^{11} \Omega$ resistors, an appropriate calibration of resistor DAC values is necessary to provide optimum performance (Trinquier et al., 2013), and DAC values of 160 were found to be appropriate for our TIMS. Otherwise, full details of the analytical method can be found in Paul et al. (2015a), with the further modification of removing inter-block peak centring in order to maximise acquisition time for samples given limited analyte material. Isotope measurements on pure NIST-SRM-981 standards were started at ~ 1280 – 1330 $^\circ\text{C}$, while starting temperatures for samples were typically slightly lower at ~ 1220 – 1280 $^\circ\text{C}$, with further inter-block heating when required to sustain ion beams. A single analysis required ~ 30 min for heating and tuning, followed by ~ 48 min for measurement, including 15 blocks of 15 cycles with an integration time of 8.4 s and a wait time of 3 s, and half-mass baselines measured in between each

block for 31.5 s with a 5 s pre-baseline wait. The measured isotopic data were processed using an iterative solver (based on Rudge et al., 2009) that was implemented as a macro within Microsoft Excel (Paul et al., 2015a). The exponential law was applied to correct for mass fractionation and was employed on a cycle-by-cycle basis, allowing the internal precision to be assessed from $2 \text{ s.d.}/\sqrt{n}$.

Blanks were typically split into unspiked and spiked portions, as for samples, and analysed by TIMS. Due to the small ion beam sizes, these measurements were typically made using the ion counter by peak jumping in dynamic mode. That approach yields sufficiently reliable Pb concentrations by isotope dilution to assess blank levels, but Pb isotopic compositions for the blanks are only expected to be indicative, given the small ion beams and the deleterious influence of a growing or decaying beam on measurements made in dynamic mode.

3. RESULTS

3.1. Accuracy and precision of Pb isotope measurements

3.1.1. Lead standard measurements

Measured Pb isotopic compositions for the NIST-SRM-981 Pb standard are reported in Table S3 and summarised in Table 1. The NIST-SRM-981 standard data were measured on 2 ng of Pb using either $10^{11} \Omega$ or $10^{12} \Omega$ resistors for the ^{204}Pb beam, with excellent agreement between the two datasets (Table 1, Fig. 4a,b) and with published data (Galer and Abouchami, 1998; Taylor et al., 2015; Klaver et al., 2016). Using the $10^{12} \Omega$ resistor in place of the $10^{11} \Omega$ resistor improves the mean internal precision (2 s.e.) on $^{206,207,208}\text{Pb}/^{204}\text{Pb}$ (hereafter $^{20x}\text{Pb}/^{204}\text{Pb}$) from ~ 420 ppm to ~ 230 ppm for 2 ng of Pb, indicating an improvement in precision of $\sim 40\%$ (Fig. 4c). The long term external reproducibility (2 s.d.) appears to scale as ~ 2.5 times the internal precision (Fig. 4d), and is similarly improved by $\sim 40\%$ (from ~ 950 ppm to ~ 550 ppm) when using the $10^{12} \Omega$ resistor in place of the $10^{11} \Omega$ resistor (Table 1). For the beam sizes obtained from 2 ng of Pb, Johnson noise (rather than counting statistics) is the dominant source of analytical uncertainty (Fig. 4c). Given potential enhancement of the signal-to-noise ratio by a factor of $\sqrt{10}$ with a $10^{12} \Omega$ resistor, and the dominant influence of the ^{204}Pb measurement on the precision of $^{20x}\text{Pb}/^{204}\text{Pb}$ ratios, an improvement of up to 68% in internal precision might have been expected (Trinquier et al., 2013; Koornneef et al., 2014). Although that full improvement was not achieved, the observed improvement is approximately in line with expectations from noise measurements for the resistors on our instrument ($\sim 17 \mu\text{V}$ on $10^{11} \Omega$, $\sim 11 \mu\text{V}$ on $10^{12} \Omega$) and is also comparable to other studies (e.g. John and Adkins, 2010).

We further note that since the installation of a $10^{12} \Omega$ resistor on the Imperial College TIMS in 2012/2013, Thermo Finnigan introduced a $10^{13} \Omega$ resistor (Koornneef et al., 2014). By using the $10^{13} \Omega$ resistor to measure the ^{204}Pb beam, Klaver et al. (2016) obtained a reproducibility of 90–125 ppm (2 s.d., $n = 22$) for $^{20x}\text{Pb}/^{204}\text{Pb}$ measurements on 5 ng aliquots of NIST-SRM-981. Our results on

Table 1
Summary of Pb isotope data for NIST-SRM-981 Pb standard, BCR-2 rock standard, and in-house coral standard.

Sample	NIST-SRM-981	NIST-SRM-981	BCR-2	Coral std	Coral std
Amount (ng)	2	2	2	3.1	31
Resistor (Ω)	10^{11}	10^{12}	10^{12}	10^{12}	10^{12}
Mean ^{204}Pb beam size (mV)	5.86	6.65	1.68	4.62	24.66
$^{206}\text{Pb}/^{204}\text{Pb}$	16.941	16.941	18.748	18.376	18.383
External 2 s.d.	0.015	0.008	0.027	0.018	0.005
External 2 s.d. (ppm)	884	490	1437	983	288
Internal 2 s.e. typical (ppm)	405	212	676	278	84
$^{207}\text{Pb}/^{204}\text{Pb}$	15.494	15.495	15.622	15.623	15.629
External 2 s.d.	0.015	0.009	0.018	0.015	0.004
External 2 s.d. (ppm)	956	567	1169	976	240
Internal 2 s.e. typical (ppm)	423	226	699	306	88
$^{208}\text{Pb}/^{204}\text{Pb}$	36.714	36.717	38.718	38.320	38.339
External 2 s.d.	0.038	0.022	0.051	0.043	0.012
External 2 s.d. (ppm)	1018	598	1315	1129	303
Internal 2 s.e. typical (ppm)	445	245	742	338	94
External/Internal for $^{20x}\text{Pb}/^{204}\text{Pb}$	2.3	2.4	1.9	3.4	3.1
Number of analyses (n)	89	47	10	10	13

Mean ^{204}Pb beam size is reported throughout as though measured on a $10^{11} \Omega$ resistor.

2 ng Pb standards are consistent with that study, although the $10^{13} \Omega$ resistor clearly offers the potential for improved precision over the $10^{12} \Omega$ resistor. Klaver et al. (2016) also suggested that the differential response and decay times of the different resistors may represent an additional challenge to obtaining accurate data, although such an effect is expected to be less significant for a $10^{12} \Omega$ resistor than for a $10^{13} \Omega$ resistor. Given the excellent agreement between standard measurements using $10^{11} \Omega$ and $10^{12} \Omega$ resistors for the ^{204}Pb beam (Table 1), and the comparable scaling between internal precision and external reproducibility in both cases (Fig. 4d), there is no indication that such an effect is influencing the accuracy or precision of the data presented here.

3.1.2. Rock and coral standard measurements

Accuracy and reproducibility of our full method (including digestion and column chemistry) is assessed based on BCR-2 rock standard and in-house coral standard data, measured using the $10^{12} \Omega$ resistor (Table S3, Table 1). For a 2 ng BCR-2 standard, typical internal precision on $^{20x}\text{Pb}/^{204}\text{Pb}$ is ~ 700 ppm (2 s.e.) and external reproducibility (2 s.d.) is ~ 1300 ppm. Those data are less precise than for a 2 ng NIST-SRM-981 standard, in part reflecting chemistry yields of $\sim 75\%$, so that only ~ 1.5 ng was available for isotope analysis, but mostly reflecting poorer ionisation (by a factor of three) for the BCR-2 standards. The beam sizes obtained for ^{204}Pb were therefore only $\sim 1\text{--}3$ mV (mean 1.7 mV) for ~ 1.5 ng BCR-2, in comparison to beam sizes of $\sim 2\text{--}15$ mV (mean 6.7 mV) for 2 ng NIST-SRM-981 (note that all signals are gain-corrected in the Thermo software as though measured on a $10^{11} \Omega$ resistor and we report ^{204}Pb beam sizes in this way throughout). Despite the small beam sizes which limit the precision of our BCR-2 measurements, the measured Pb isotope values are in excellent agreement with literature data measured on larger quantities of Pb (e.g. Woodhead and Hergt, 2000; Weis et al.,

2006; Todd et al., 2015), indicating the accuracy of our method for small quantities of Pb.

For our in-house coral standard, we obtain chemistry yields of typically 80–95% (Table S3), and somewhat better ionisation than for the BCR-2 standard (i.e., only a factor of two poorer than for NIST-SRM-981 standards; Table 1). Lead isotope data from both 3.1 ng and 31 ng coral standards agree within error. For the 3.1 ng coral standards, the typical internal precision on $^{20x}\text{Pb}/^{204}\text{Pb}$ is ~ 300 ppm (2 s.e.), with external reproducibility (2 s.d.) of ~ 1000 ppm (Table 1). Similar relationships between beam size and internal precision, and between internal precision and external reproducibility, apply to the coral standard as for the pure NIST-SRM-981 standard (Fig. 4c,d). The external reproducibility is around 3 times the internal precision, which is only a slightly larger scaling than for the pure NIST-SRM-981 standards (Fig. 4d, Table 1), constraining any variable matrix effect or blank effect from the digestion and chemistry steps to be minimal. Therefore, we use this 3:1 relationship to provide an estimate of the likely external reproducibility of Pb isotopic composition measurements on unknown coral samples based on their internal precision (e.g. Bizzarro et al., 2003; Todd et al., 2015). In addition, we note that Pb isotope measurements on the coral standards from our column yield test (Fig. 3) agree within their expected external reproducibility over the observed range of yields from $\sim 50\text{--}90\%$ (Table S3), indicating that mass fractionation occurring on the columns (i.e., before spiking) is negligible (see also Fig. 1 of Paul et al., 2015a).

3.1.3. Lead blanks

Full procedural blanks, including chemical cleaning, digestion, two-step column chemistry, loading and measurement, were typically $\sim 20\text{--}40$ pg, reflecting careful laboratory protocols developed over the course of the study. In detail, blanks for one-step column chemistry were 6 ± 1 pg (1 s.d., $n = 6$); blanks for the complete column chemistry

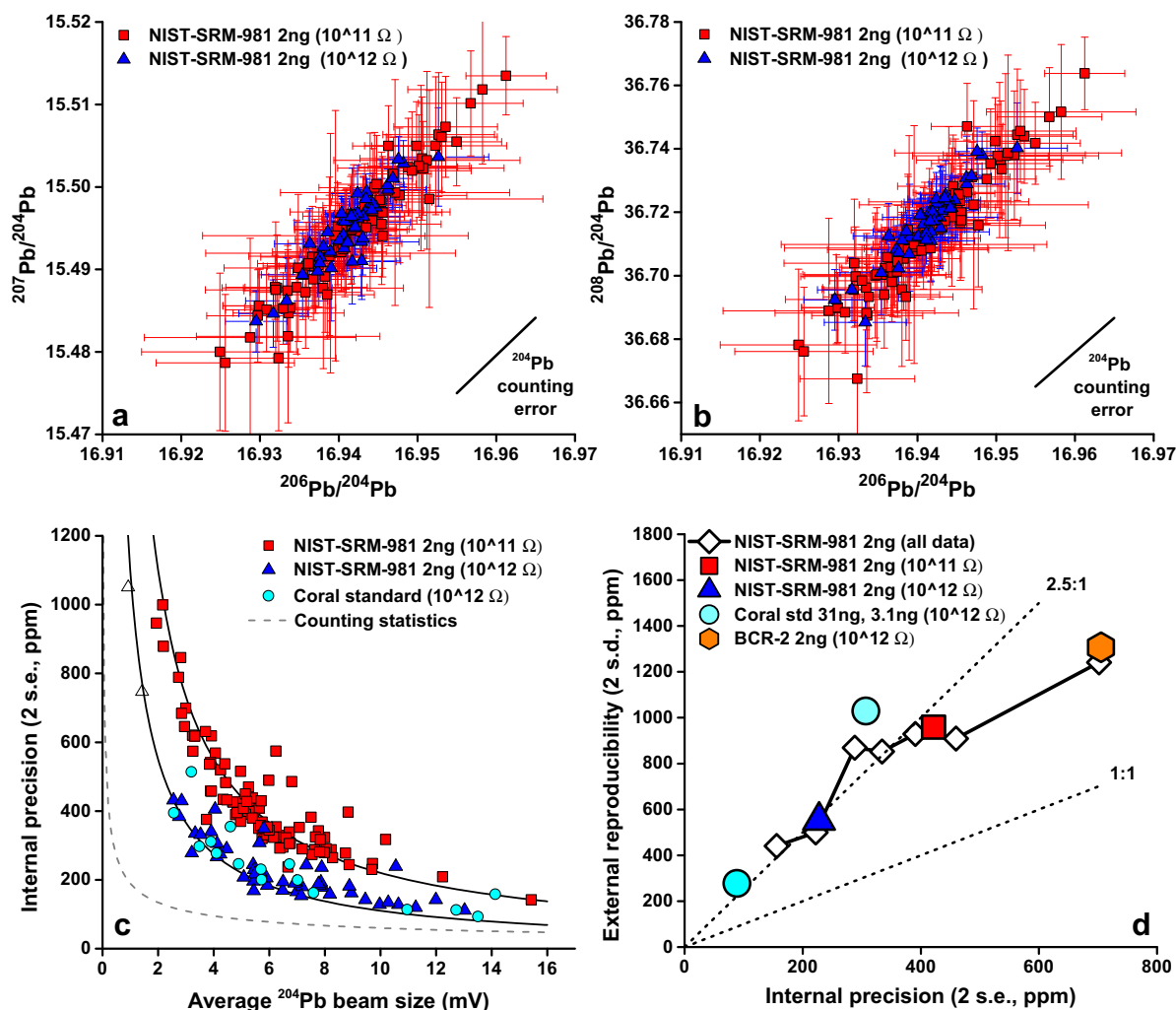


Fig. 4. Evaluation of precision and accuracy of TIMS measurements. (a) $^{207}\text{Pb}/^{204}\text{Pb}$ versus $^{206}\text{Pb}/^{204}\text{Pb}$ for NIST-SRM-981 Pb standard, measured using either $10^{11}\ \Omega$ or $10^{12}\ \Omega$ resistors for the ^{204}Pb beam. (b) $^{208}\text{Pb}/^{204}\text{Pb}$ versus $^{206}\text{Pb}/^{204}\text{Pb}$ for NIST-SRM-981 Pb standard. (c) Internal precision (2 s.e.) on $^{207}\text{Pb}/^{204}\text{Pb}$ as a function of average beam size on ^{204}Pb for the unspiked run, plotted for both the NIST-SRM-981 Pb standard and our in-house coral standard. The dashed curve indicates the theoretical precision from counting statistics alone (John and Adkins, 2010), based only on the unspiked run which represents the main source of uncertainty. The measured data lie significantly above that curve, indicating that Johnson noise is the predominant control on internal precision for this range of beam sizes. The solid curves are indicative fits through the data and indicate the improvement in precision when using the $10^{12}\ \Omega$ (versus $10^{11}\ \Omega$) resistor. Measurements of our in-house coral standard (typically 3.1 ng, but a few larger samples are included) indicate quite comparable behaviour to the NIST-SRM-981 standards. Note that two measurements with very poor beam intensities (open triangles) are included in this plot to demonstrate the internal precision as a function of beam size, but are otherwise excluded from our statistics. (d) Relationship between internal precision and external reproducibility on $^{207}\text{Pb}/^{204}\text{Pb}$, for NIST-SRM-981 Pb standard, in-house coral standard and BCR-2 rock standard. For the line (with diamond symbols), all individual NIST-SRM-981 Pb analyses (Table S3) were ordered by their internal precision, grouped into sets of 20 analyses (or 16 for the final data point), and both the average internal precision (2 s.e.) and the external reproducibility (2 s.d.) of the 20 analyses were calculated. Data points based on the full datasets of various standards (individual large symbols) are also shown based on data in Table 1. Dotted lines show indicative 1:1 and 2.5:1 lines, with external reproducibility generally scaling as approximately 2.5 times the internal precision for the NIST-SRM-981 standards. Data from the coral and BCR-2 standards are quite consistent with the relationship shown for the NIST-SRM-981 standards.

procedure were $17 \pm 3\ \text{pg}$ ($n = 8$); blanks for digestion and complete column chemistry were $24 \pm 9\ \text{pg}$ ($n = 7$); and blanks for chemical cleaning, digestion and complete column chemistry were $29 \pm 9\ \text{pg}$ ($n = 6$). Those blanks are comparable to blank levels reported in the seawater studies of Paul et al. (2015a) that were carried out in the same laboratories. Isotopic measurements of the blanks are not very

reproducible ($^{206}\text{Pb}/^{204}\text{Pb} = 18.4 \pm 0.9$; $^{207}\text{Pb}/^{204}\text{Pb} = 15.2 \pm 0.7$; $^{208}\text{Pb}/^{204}\text{Pb} = 37.2 \pm 1.8$; $n = 17$; 1 s.d.), which may reflect in part the inherent uncertainty of measuring small and declining ion beams using the ion counter, but could also represent true variability in blank compositions.

For the deglacial coral samples, the expected blank contribution represents ~ 0.03 –2% of our measured Pb.

Considering a representative deglacial sample yielding ~ 8 ng of Pb, a maximum blank of ~ 40 pg would contribute $\sim 0.5\%$ of the measured Pb. Based on the above reported isotopic composition of the blank, we estimate a possible offset to the measured sample values of ~ 0.002 for $^{206}\text{Pb}/^{204}\text{Pb}$ (~ 100 ppm), ~ 0.002 for $^{207}\text{Pb}/^{204}\text{Pb}$ (~ 150 ppm), and ~ 0.008 for $^{208}\text{Pb}/^{204}\text{Pb}$ (~ 200 ppm). Given that these values are comparable to the internal precision of our measurements, and since the blank composition itself appears highly variable, no blank correction is applied. Even for our smallest deglacial coral sample (T20, yielding only ~ 1.7 ng of Pb), offsets due to a blank contribution are likely to be no more than ~ 0.01 for $^{206}\text{Pb}/^{204}\text{Pb}$ (~ 500 ppm), ~ 0.01 for $^{207}\text{Pb}/^{204}\text{Pb}$ (~ 700 ppm), and ~ 0.04 for $^{208}\text{Pb}/^{204}\text{Pb}$ (~ 900 ppm), which are larger than the internal precision (~ 400 ppm) but comparable to the estimated external reproducibility (~ 1200 ppm) for such a sample.

We note here that during analyses of samples A–E from our cleaning experiment, blank levels were in the range of 150–330 pg and hence a lot higher than the long term values. The problem could largely be attributed to a contaminated source of concentrated HBr, and all our subsequent work was carried out using Suprapure/Optima grade HBr. Fortunately, the very high Pb concentrations of the coral samples in the cleaning experiment yielded 50–150 ng of Pb per sample, resulting in blank contributions of $\sim 0.5\%$ or less, which would contribute to offsets smaller than 200 ppm in all measured ratios.

3.2. Coral cleaning experiments

The Pb isotope results of our cleaning experiment are reported in Table 2 and plotted in Fig. 5. Replicate mass spectrometry measurements on aliquots of the same portion of fully cleaned coral (samples A.2a–d) agree within error. Chemistry replicates (i.e., samples A.1, A.2, A.3) and full procedural replicates on separate pieces of coral (i.e., samples A, B, C) also agree within error, with an overall mean $^{206}\text{Pb}/^{204}\text{Pb} = 18.768 \pm 0.013$ (2 s.d.; $n = 6$; omitting here the measurements on aliquots of only ~ 1.5 ng Pb), indicating a reproducibility of ~ 700 ppm. That calculation includes samples where an aqua regia step was included during digestion (sample A.3), which had no noticeable effect on the Pb isotopic compositions, and where the coral fragments were crushed to a fine sand before cleaning (sample C), where there was possibly a minor offset, but not significantly larger than the difference between samples A and B. Excluding sample C, so that all samples underwent essentially the same physical and chemical treatment, leads to a reproducibility of ~ 420 ppm (2 s.d.; $n = 5$).

The Pb isotope results for sample F, which underwent physical cleaning and minor chemical rinsing steps (but not the full chemical cleaning procedure), also agree with the fully cleaned samples A–C (Fig. 5a,b). In contrast, sample E, which underwent no physical cleaning and only minor chemical rinsing steps (i.e., it is basically uncleaned), has a significantly different composition of $^{206}\text{Pb}/^{204}\text{Pb} = 18.210 \pm 0.001$ (2 s.e.), which is offset by $\sim 30,000$ ppm from the cleaned samples (Fig. 5c,d). Sample

D, which underwent no physical cleaning but was subjected to the full chemical cleaning procedure, has a composition of $^{206}\text{Pb}/^{204}\text{Pb} = 18.703 \pm 0.009$ (2 s.e.), which is intermediate on a mixing line between the cleaned and uncleaned samples, although significantly closer to the cleaned samples (Fig. 5a,b).

Estimated Pb concentrations in the chemically cleaned samples (samples A–D) were ~ 280 – 360 ppb (Pb/Ca ~ 130 – 170 nmol/mol), compared to ~ 1000 ppb (Pb/Ca ~ 480 nmol/mol) in the uncleaned sample (sample E). These values all represent minimum estimates because they were calculated based on cuts taken after column chemistry, and for the sample sizes processed in the cleaning experiments we do not expect to have achieved 100% yields (Fig. 3). Nevertheless, these results suggest that ~ 60 – 70% of the total Pb associated with this uncleaned coral was removed by the combined physical and chemical cleaning procedure. Sample F (i.e., physically cleaned and rinsed) had a significantly lower Pb concentration of ~ 90 ppb (Pb/Ca ~ 45 nmol/mol) than the other samples, perhaps due to sampling from near the base of the coral rather than from the septae (pointing to complex controls on the Pb distribution in corals), but its Pb isotopic composition is identical to the fully cleaned corals.

3.3. Deglacial Pb isotope record from Tasmania

Lead isotope measurements on the suite of glacial and deglacial corals (Table 3) are shown in Pb–Pb crossplots (Fig. 6) and as a time series of $^{206}\text{Pb}/^{204}\text{Pb}$ (Fig. 7). Typical Pb concentrations for the cleaned deglacial samples were ~ 6 – 20 ppb (Pb/Ca ~ 3 – 10 nmol/mol), yielding ~ 3 – 10 ng of Pb for isotope analysis. In a few cases, much higher concentrations of ~ 40 – 80 ppb (Pb/Ca ~ 20 – 40 nmol/mol), and in one case nearly 200 ppb (Pb/Ca ~ 100 nmol/mol) were observed (Table 3), resulting in significantly greater amounts of Pb for analysis. Therefore, our NIST-SRM-981 (2 ng) and in-house coral standards (3.1 ng, 31 ng) are quite appropriate for comparison to the measured coral data. Although a few samples have significantly higher Pb concentrations, their Pb isotopic compositions are not distinct from the low concentration samples, and no relationship between Pb concentrations and Pb isotopic compositions was detected in the full dataset.

The Pb–Pb crossplots (Fig. 6) demonstrate a very close linear relationship between $^{206}\text{Pb}/^{204}\text{Pb}$ and $^{208}\text{Pb}/^{204}\text{Pb}$ ratios ($r^2 \sim 0.97$), which is also the case if a ratio involving ^{204}Pb is plotted against an independent ratio not including ^{204}Pb (e.g. $^{206}\text{Pb}/^{204}\text{Pb}$ versus $^{208}\text{Pb}/^{207}\text{Pb}$; $r^2 \sim 0.99$; not shown). Taken together, these observations provide strong support for the accuracy of our measurements, including the minor ^{204}Pb isotope. In addition, the gradient of the correlation between $^{206}\text{Pb}/^{204}\text{Pb}$ and $^{208}\text{Pb}/^{204}\text{Pb}$ (Fig. 6b) is inconsistent with that expected for either uncorrected mass bias or ^{204}Pb counting error, and appears to represent a binary mixing relationship. Furthermore, the excellent correlation in Pb–Pb space holds up, no matter whether internal precision or external reproducibility are considered (Fig. 6b). Variability in $^{207}\text{Pb}/^{204}\text{Pb}$ is less well resolved than for the other ratios (Fig. 6a), reflecting the more

Table 2
Lead isotope data from coral cleaning experiment.

Lab code	Cleaning	Weight loss (%)	Minimum [Pb] (ng/g)	$^{206}\text{Pb}/^{204}\text{Pb}$	2 s.e.	$^{207}\text{Pb}/^{204}\text{Pb}$	2 s.e.	$^{208}\text{Pb}/^{204}\text{Pb}$	2 s.e.	$^{206}\text{Pb}/^{207}\text{Pb}$	2 s.e.	$^{208}\text{Pb}/^{207}\text{Pb}$	2 s.e.	$^{208}\text{Pb}/^{206}\text{Pb}$	2 s.e.	Amount run (ng)	Mean ^{204}Pb beam (V)
A.1	Full cleaning	7	340	18.7675	0.0007	15.6575	0.0006	38.7703	0.0016	1.19863	0.00001	2.47618	0.00002	2.06583	0.00002	91.1	0.075
A.2a	Full cleaning [1]	7	313	18.7651	0.0014	15.6548	0.0013	38.7630	0.0032	1.19867	0.00002	2.47614	0.00004	2.06572	0.00004	46.3	0.024
A.2b	Full cleaning [1]	n.a.	n.a.	18.7667	0.0016	15.6558	0.0013	38.7658	0.0033	1.19871	0.00002	2.47615	0.00004	2.06567	0.00003	42.2	0.017
A.2c	Full cleaning [1]	n.a.	n.a.	18.7300	0.0244	15.6230	0.0207	38.6745	0.0559	1.19880	0.00025	2.47621	0.00046	2.06544	0.00057	1.3	0.001
A.2d	Full cleaning [1]	n.a.	n.a.	18.7615	0.0144	15.6441	0.0125	38.7500	0.0337	1.19917	0.00019	2.47683	0.00037	2.06548	0.00052	1.4	0.001
A.3	Full cleaning [2]	7	291	18.7596	0.0005	15.6559	0.0005	38.7588	0.0015	1.19825	0.00001	2.47568	0.00002	2.06608	0.00003	92.8	0.114
B	Full cleaning [3]	8	323	18.7701	0.0016	15.6602	0.0019	38.7791	0.0064	1.19860	0.00005	2.47622	0.00011	2.06592	0.00018	139.6	0.136
C	Full cleaning [4]	27	364	18.7798	0.0006	15.6554	0.0005	38.7795	0.0015	1.19957	0.00001	2.47704	0.00003	2.06494	0.00002	89.7	0.086
D	Chemical only	13	284	18.7030	0.0092	15.6392	0.0077	38.6837	0.0187	1.19593	0.00009	2.47348	0.00017	2.06820	0.00011	61.4	0.002
E	Uncleaned	6	974	18.2101	0.0008	15.6129	0.0008	38.1466	0.0019	1.16635	0.00001	2.44327	0.00003	2.09478	0.00003	86.9	0.035
F	Physical only	10	92	18.7709	0.0017	15.6560	0.0015	38.7659	0.0039	1.19895	0.00002	2.47601	0.00004	2.06517	0.00006	14.8	0.025

Errors on Pb isotope measurements represent internal precision (2 s.e.).

External reproducibility (2 s.d.) for $^{208}\text{Pb}/^{204}\text{Pb}$ is likely to be around 3 times internal precision (see discussion in text).

All measurements were made using the $10^{12} \Omega$ resistor for the unspiked run, except for sample F.

Weight loss reports loss during chemical cleaning procedure.

[1]: Chemistry replicate.

[2]: Chemistry replicate with aqua regia step.

[3]: Full procedural replicate.

[4]: Full procedural replicate with crushing.

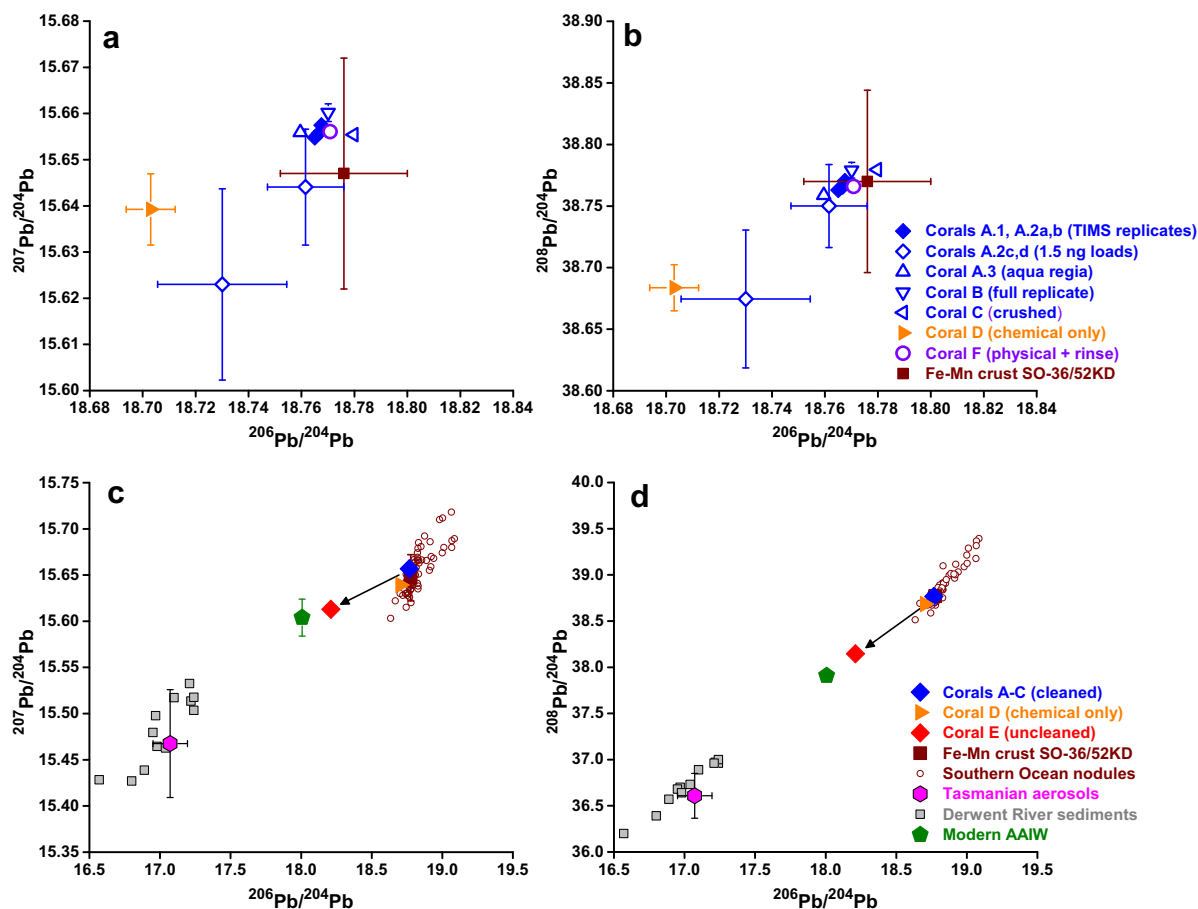


Fig. 5. Lead isotope results from the coral cleaning experiment, plotted as (a,c) $^{207}\text{Pb}/^{204}\text{Pb}$ versus $^{206}\text{Pb}/^{204}\text{Pb}$, and (b,d) $^{208}\text{Pb}/^{204}\text{Pb}$ versus $^{206}\text{Pb}/^{204}\text{Pb}$. (a,b) Detailed view of data from coral cleaning experiments A, B, C, D and F compared to the composition of the most proximal ferromanganese crust SO-36/52KD (46°S, 147°E, 1.7 km depth; von Blanckenburg et al., 1996). (c,d) Data from coral cleaning experiments A–C (combined), D and E compared to potential Pb sources. Southern Ocean ferromanganese crusts and nodules (Abouchami and Goldstein, 1995; von Blanckenburg et al., 1996; Vlastelic et al., 2001) provide evidence on the likely pre-anthropogenic compositions of seawater in the Southern Ocean (Fig. 1). The compositions of Tasmanian aerosols (Bollhofer and Rosman, 2000), recent sediments from the Derwent River, Tasmania (Townsend and Seen, 2012), and modern AAIW (South Atlantic; cruise D357, sample 3–169, 36°S, 13°E, ~1 km depth; Paul et al., 2015a) represent likely anthropogenic sources in the region (Fig. 1). Error bars for the coral data (only shown where larger than the data points) represent internal precision (2 s.e.), whereas external reproducibility is likely ~3 times larger (see Fig. 4d). For literature data, external reproducibility (2 s.d.) is plotted for AAIW and SO-36/52KD, the Tasmanian aerosol data are represented by the mean and range of two measurements, while for clarity uncertainties are not plotted for the fields of Southern Ocean nodules or Derwent River sediments.

limited ^{207}Pb variability in the natural environment, but remains consistent with those interpretations. In addition, full procedural replicate analyses of sample T24, incorporating both procedural reproducibility and potential sample heterogeneity, are in agreement (Table 3) when considering external reproducibility (calculated as 3 times internal precision). Therefore, both the precision of our measurements and the reproducibility of the method appear suitable to resolve variability in the Pb isotopic composition of the coral skeletons.

Considering the temporal changes recorded by the suite of corals (Fig. 7), there is high frequency variability on (sub-)millennial timescales, but no overall secular trend. In particular, based on the corals from 1.44 to 1.69 km water depth, the mean compositions during the last glacial period (~25–40 ka; $^{206}\text{Pb}/^{204}\text{Pb} = 18.76 \pm 0.02$, 1 s.d.),

the Last Glacial Maximum (~17–23 ka; $^{206}\text{Pb}/^{204}\text{Pb} = 18.75 \pm 0.03$, 1 s.d.), and the Antarctic Cold Reversal (~12–14.6 ka; $^{206}\text{Pb}/^{204}\text{Pb} = 18.73 \pm 0.06$, 1 s.d.) are indistinct in comparison to the range of variability recorded within any of these time periods.

4. DISCUSSION

4.1. Recovering seawater Pb isotopes from deep-sea corals

The key advance from our analytical method development is the improved ability to resolve Pb isotope variability in sample sizes of 2–10 ng Pb. Whereas previous studies on marine carbonates have typically not reported the minor ^{204}Pb isotope (e.g. Reuer et al., 2003; Kelly et al., 2009; Lee et al., 2017), here we take advantage of a double-spike

Table 3
Lead isotope data from deglacial corals.

Lab code	Sample name	Depth (m)	Age (ka BP)	2 σ	Weight loss (%)	Minimum [Pb] (ng/g)	²⁰⁶ Pb/ ²⁰⁴ Pb	2 s.e.	²⁰⁷ Pb/ ²⁰⁴ Pb	2 s.e.	²⁰⁸ Pb/ ²⁰⁴ Pb	2 s.e.	²⁰⁶ Pb/ ²⁰⁷ Pb	2 s.e.	²⁰⁸ Pb/ ²⁰⁷ Pb	2 s.e.	²⁰⁸ Pb/ ²⁰⁶ Pb	2 s.e.	Amount run (ng)	Mean ²⁰⁴ Pb beam (V)
T9	TN228-J2-393-0112-0730-13-1442-008	1442	12.21	0.13	9	12.9	18.7266	0.0033	15.6532	0.0029	38.7433	0.0075	1.19628	0.00005	2.47497	0.00009	2.06888	0.00010	3.3	0.006
T16	TN228-J2-387-1226-1635-23-1599-014	1599	13.35	0.03	10	7.3	18.7886	0.0041	15.6577	0.0034	38.8009	0.0089	1.20000	0.00005	2.47813	0.00009	2.06509	0.00012	3.9	0.005
T15	TN228-J2-387-1226-1635-23-1599-003	1599	13.62	0.08	10	12.0	18.7398	0.0023	15.6517	0.0020	38.7409	0.0050	1.19730	0.00003	2.47520	0.00006	2.06733	0.00007	4.4	0.009
T10 [*]	TN228-J2-395-0113-1830-05-1947-003	1947	13.71	0.16	7	7.8	18.5087	0.0046	15.6383	0.0037	38.4984	0.0099	1.18355	0.00006	2.46182	0.00010	2.08002	0.00011	3.3	0.004
T11 [*]	TN228-J2-387-1225-1253-11-1898-001	1898	14.38	0.05	16	6.6	18.8001	0.0041	15.6605	0.0037	38.8164	0.0101	1.20057	0.00006	2.47858	0.00012	2.06449	0.00017	2.8	0.005
T17	TN228-J2-387-1226-1635-23-1599-016	1599	14.39	0.08	8	8.8	18.6481	0.0034	15.6404	0.0030	38.6288	0.0078	1.19228	0.00005	2.46994	0.00009	2.07159	0.00010	3.0	0.006
T18	TN228-J2-387-1226-1507-22-1616-004	1616	14.83	0.03	11	35.5	18.7318	0.0017	15.6511	0.0019	38.7303	0.0058	1.19686	0.00004	2.47462	0.00009	2.06760	0.00015	14.3	0.026
T19	TN228-J2-382-1216-1010-01-1689-004	1689	17.28	0.11	8	5.8	18.7739	0.0081	15.6578	0.0068	38.7747	0.0167	1.19903	0.00010	2.47646	0.00018	2.06539	0.00018	3.0	0.003
T20	TN228-J2-382-1216-1010-01-1689-009	1689	17.61	0.16	17	9.4	18.7381	0.0075	15.6463	0.0067	38.7335	0.0173	1.19753	0.00009	2.47531	0.00015	2.06695	0.00018	1.6	0.003
T21	TN228-J2-382-1216-1350-03-1523-007	1523	18.33	0.04	8	13.7	18.6817	0.0012	15.6472	0.0011	38.6772	0.0029	1.19392	0.00002	2.47180	0.00004	2.07033	0.00006	7.4	0.022
T22	TN228-J2-383-1217-1320-05-1460-009	1460	19.48	0.06	13	72.6	18.7492	0.0015	15.6516	0.0013	38.7410	0.0035	1.19792	0.00002	2.47520	0.00004	2.06625	0.00005	32.9	0.018
T23 [#]	TN228-J2-383-1217-0725-01-1575-023	1575	19.79	0.19	7	16.5	18.7374	0.0025	15.6549	0.0023	38.7496	0.0061	1.19695	0.00003	2.47530	0.00007	2.06800	0.00008	8.7	0.009
T25 [#]	TN228-J2-382-1216-1350-03-1523-005	1523	21.40	0.18	7	15.0	18.7702	0.0033	15.6549	0.0030	38.7815	0.0076	1.19898	0.00004	2.47713	0.00008	2.06598	0.00008	7.7	0.007
T24	TN228-J2-382-1216-1350-03-1523-003	1523	21.70	0.16	7	15.7	18.7804	0.0030	15.6558	0.0027	38.7915	0.0076	1.19964	0.00005	2.47784	0.00008	2.06554	0.00012	8.1	0.008
T24 rep	TN228-J2-382-1216-1350-03-1523-003	1523	21.70	0.16	9	11.3	18.7655	0.0042	15.6456	0.0039	38.7549	0.0100	1.19942	0.00006	2.47725	0.00010	2.06531	0.00010	5.6	0.006
T26	TN228-J2-395-0114-0057-09-1500-010	1500	25.20	0.14	15	16.8	18.7892	0.0025	15.6572	0.0022	38.7968	0.0056	1.20002	0.00003	2.47785	0.00006	2.06486	0.00007	7.0	0.009
T27	TN228-J2-383-1217-0725-01-1575-017	1575	26.19	0.06	33	34.4	18.7422	0.0025	15.6485	0.0023	38.7344	0.0060	1.19768	0.00004	2.47533	0.00008	2.06673	0.00010	4.3	0.009
T28	TN228-J2-395-0114-0057-09-1500-003	1500	30.77	0.19	9	63.8	18.7562	0.0009	15.6556	0.0008	38.7675	0.0023	1.19807	0.00002	2.47628	0.00003	2.06688	0.00004	31.4	0.032
T30	TN228-J2-383-1217-0725-01-1575-007	1575	31.29	0.17	10	29.7	18.7472	0.0019	15.6473	0.0017	38.7332	0.0044	1.19813	0.00003	2.47541	0.00005	2.06609	0.00006	13.7	0.012
T33	TN228-J2-383-1217-0725-01-1575-009	1575	32.25	0.12	8	18.0	18.7555	0.0018	15.6480	0.0015	38.7302	0.0038	1.19861	0.00002	2.47509	0.00004	2.06494	0.00004	7.9	0.013
T31 [#]	TN228-J2-383-1217-0725-01-1575-025	1575	32.71	0.36	8	54.5	18.7771	0.0009	15.6525	0.0008	38.7740	0.0021	1.19965	0.00002	2.47717	0.00003	2.06492	0.00003	24.9	0.031
T29	TN228-J2-382-1216-1010-01-1689-007	1689	34.36	0.16	9	15.1	18.7664	0.0041	15.6526	0.0035	38.7760	0.0090	1.19892	0.00006	2.47724	0.00008	2.06632	0.00007	6.4	0.004
T32	TN228-J2-393-0112-0124-06-1657-004	1657	36.33	0.11	7	16.4	18.7314	0.0021	15.6491	0.0018	38.7185	0.0048	1.19702	0.00003	2.47424	0.00006	2.06703	0.00006	7.6	0.010
T13 ^s	TN228-J2-386-1223-0739-07-0958-001	958	36.42	0.24	15	47.8	18.7746	0.0014	15.6586	0.0014	38.7861	0.0042	1.19897	0.00003	2.47690	0.00006	2.06586	0.00009	13.8	0.021
T14 [*]	TN228-J2-393-0111-1851-02-1816-008	1816	38.66	0.09	11	26.2	18.7474	0.0016	15.6554	0.0015	38.7561	0.0042	1.19749	0.00003	2.47556	0.00006	2.06732	0.00009	9.4	0.017
T34	TN228-J2-395-0114-0057-09-1500-009	1500	39.70	0.16	18	187.5	18.7456	0.0009	15.6509	0.0009	38.7436	0.0027	1.19774	0.00002	2.47548	0.00004	2.06680	0.00007	89.5	0.079

Errors on Pb isotope measurements represent internal precision (2 s.e.).

External reproducibility (2 s.d.) for ²⁰⁸Pb/²⁰⁴Pb is likely to be around 3 times internal precision (see discussion in text).

All measurements were made using the 10¹² Ω resistor for the unspiked run.

All U–Th ages are from [Hines et al. \(2015\)](#) unless otherwise stated.

rep: Full procedural replicate for Pb isotope data.

^{*} See [Table S1](#) for U–Th dates.

[#] High ²³²Th (>2000 ppt) indicated in [Hines et al. \(2015\)](#).

^s Non-marine δ²³⁴U_i (where marine is defined as 147 ± 7 pre-17 ka and 141.7 ± 7.8 post-17 ka by IntCal09).

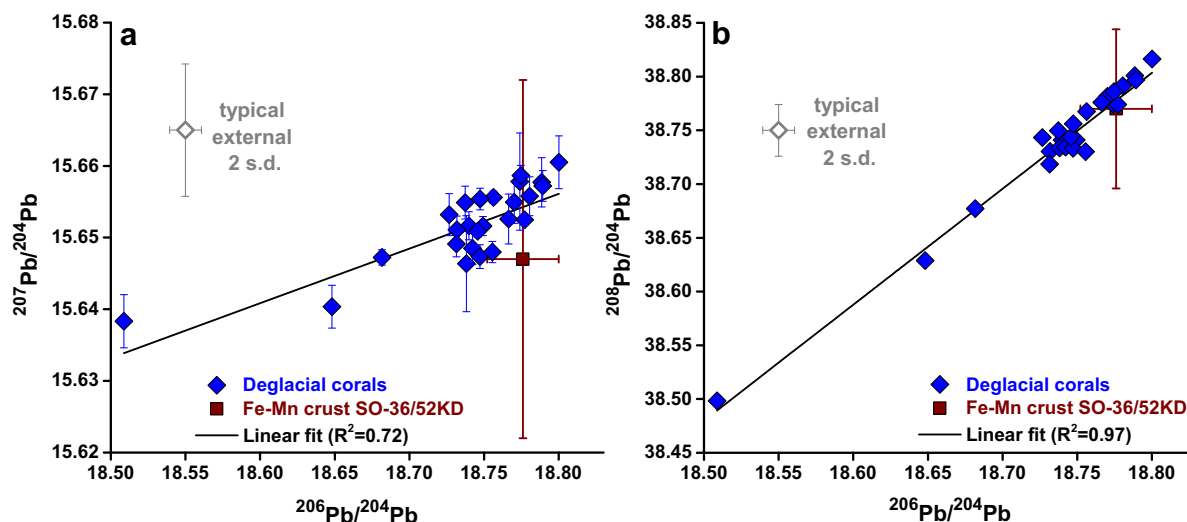


Fig. 6. Late glacial and deglacial coral Pb isotope data, plotted as (a) $^{207}\text{Pb}/^{204}\text{Pb}$ versus $^{206}\text{Pb}/^{204}\text{Pb}$, and (b) $^{208}\text{Pb}/^{204}\text{Pb}$ versus $^{206}\text{Pb}/^{204}\text{Pb}$. The composition of proximal Tasmanian ferromanganese crust SO-36/52KD (46°S, 147°E, 1.7 km depth; von Blanckenburg et al., 1996) is shown for comparison. Error bars on coral data points represent internal precision (2 s.e.) for $^{207}\text{Pb}/^{204}\text{Pb}$, and are comparable to (or smaller than) symbol sizes for the other ratios. Separate error bar provides indicative external reproducibility (2 s.d.) for a typical sample (calculated as 3 times the average internal precision for sub-10 ng samples, based on the relationship in Fig. 4d). Linear best-fit lines through the coral data and their accompanying R^2 values are also reported.

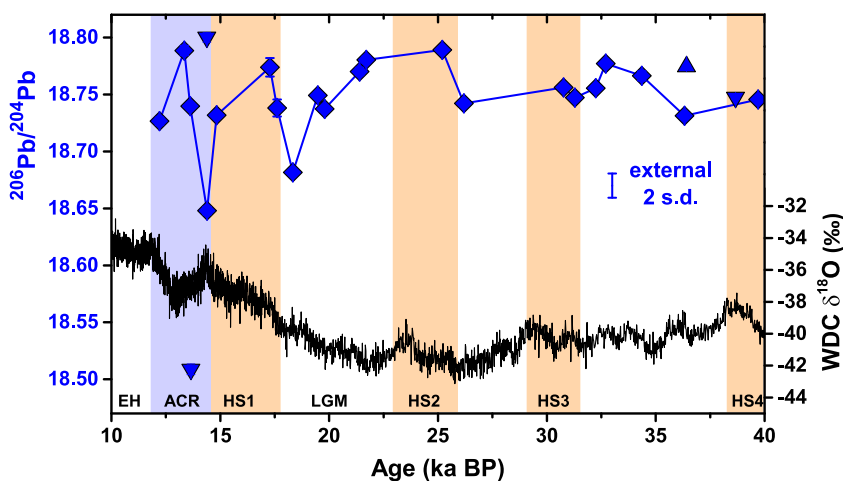


Fig. 7. Late glacial and deglacial coral Pb isotope record (plotted for $^{206}\text{Pb}/^{204}\text{Pb}$; other ratios have a similar pattern) compared to the Antarctic ice core $\delta^{18}\text{O}$ temperature proxy record from WAIS Divide Core (WDC; Buizert et al., 2015). The majority of coral samples are from 1.44–1.69 km water depth and those data are connected by a line. Deeper samples (1.82–1.95 km; downward triangles) and shallower sample (0.96 km; upward triangle) are plotted separately. Error bars on coral data represent internal precision (2 s.e.) and are only shown where larger than symbol sizes. Separate error bar provides indicative external reproducibility (2 s.d.) for a typical sample (as described in Fig. 6 caption). Uncertainties in coral ages are smaller than symbol sizes. Time intervals are labelled along the x axis: ACR = Antarctic Cold Reversal; EH = Early Holocene; HS = Heinrich Stadial; LGM = Last Glacial Maximum.

TIMS method combined with a $10^{12} \Omega$ resistor for the ^{204}Pb beam to measure $^{208}\text{Pb}/^{204}\text{Pb}$ ratios on deep-sea corals with a typical internal precision of ~ 200 ppm (2 s.e.) and external reproducibility (2 s.d.) of ~ 600 ppm (Fig. 6). Therefore, we are able to apply our method to corals that grew in the pre-anthropogenic era with low seawater Pb concentrations. The overall variability (i.e., range) in our deglacial

coral dataset is $\sim 15,000$ ppm for $^{206}\text{Pb}/^{204}\text{Pb}$ (Fig. 7), or ~ 8000 ppm when excluding one particularly unradiogenic sample (T10), indicating that the natural signal exceeds measurement uncertainty by an order of magnitude.

In addition to requiring accurate and precise Pb isotope measurements, our cleaning experiment demonstrates that physical and chemical cleaning of coral skeletons is critical

for reliably recovering past seawater compositions from deep-sea corals (Fig. 5). In interpreting those results, we use ferromanganese crusts and nodules to provide evidence on the local pre-anthropogenic seawater Pb isotopic composition in the Southern Ocean (Abouchami and Goldstein, 1995; von Blanckenburg et al., 1996; Vlastelic et al., 2001), and the compositions of local Tasmanian aerosols (Bollhofer and Rosman, 2000) and modern Tasmanian river sediments (Townsend and Seen, 2012) to represent anthropogenic Pb contaminants to this region of the Southern Ocean. Comparison to these compositions indicates that the uncleaned coral (sample E) is strongly influenced by an unradiogenic anthropogenic Pb contaminant (Fig. 5c,d). In contrast, the Pb isotopic compositions of the fully cleaned corals (i.e., samples A-C) and the physically cleaned and rinsed coral (sample F) are consistent with the local pre-anthropogenic seawater composition (Fig. 5a,b).

Although surface anthropogenic Pb contamination of the uncleaned coral (sample E) could potentially have occurred during shipboard collection or laboratory sampling, we suggest instead that this Pb may represent a layer of anthropogenic Pb that was acquired post-mortem from the modern water column, through processes such as surface adsorption or the formation of an organic or oxide coating. Based on recent observations of a significant anthropogenic Pb isotope imprint in modern day Southern Ocean intermediate water masses (Lee et al., 2015; Paul et al., 2015a), the modern day AAIW composition would appear to represent a suitable unradiogenic endmember

for the uncleaned coral sample (Fig. 5c,d). If that modern AAIW composition is taken to be representative of the Pb recently added to the coral, mass balance constraints (taking into account both Pb isotopes and the ~60–70% Pb loss between uncleaned and cleaned samples; Section 3.2) would indicate that the full cleaning procedure is removing all of the recent Pb and very little of the natural Pb present in the corals.

To summarise, our cleaning experiment highlights that physical cleaning is the most important step for producing reproducible Pb isotope results, and that physical cleaning combined with chemical rinsing may be sufficient (Fig. 5). Nevertheless, for consistency with other studies on deep-sea corals, such as those measuring Nd isotopes (van de Flierdt et al., 2010; Crocket et al., 2014), we continued to apply full physical and chemical cleaning to all samples. As for the cleaned coral data from the cleaning experiment, the Pb isotope data collected from the cleaned deglacial corals also largely overlap with the compositions of Southern Ocean ferromanganese crusts, whereas they are quite distinct from the composition of the uncleaned coral (Fig. 8). Since the observations from the cleaning experiment seem to apply to this larger sample set, and given a hydrogenous origin for ferromanganese crusts, the deglacial data further support that dissolved Pb in seawater represents the main source of Pb in cleaned corals.

Finally, we consider the evidence from Pb concentrations in the cleaned corals. The majority of the deglacial corals have relatively low Pb concentrations in the order of 6–20 ppb (Pb/Ca ~3–10 nmol/mol), as might be

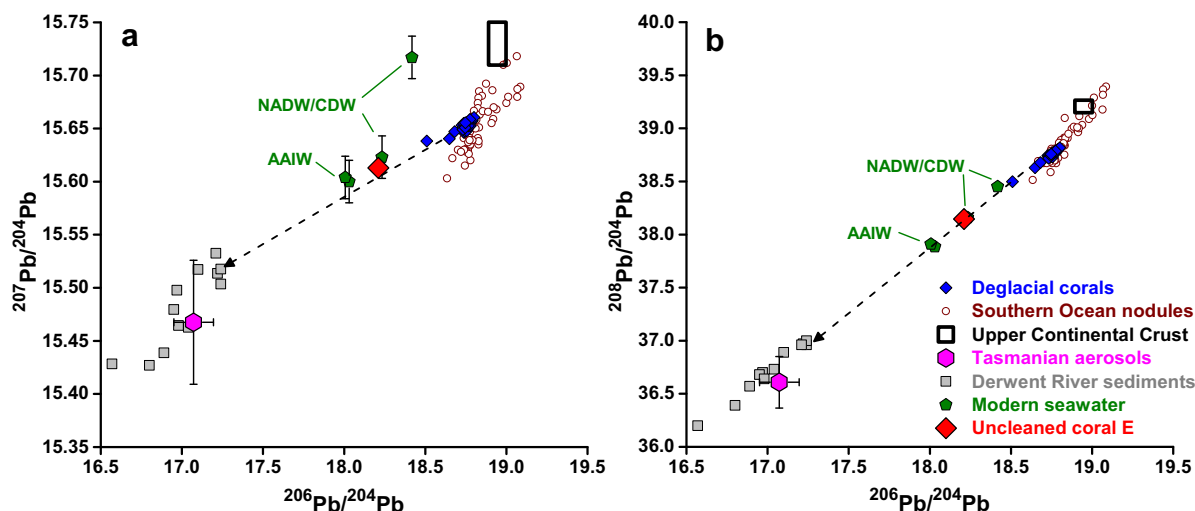


Fig. 8. Potential sources of anthropogenic versus natural Pb to the glacial and deglacial corals, assessed from (a) $^{207}\text{Pb}/^{204}\text{Pb}$ versus $^{206}\text{Pb}/^{204}\text{Pb}$, and (b) $^{208}\text{Pb}/^{204}\text{Pb}$ versus $^{206}\text{Pb}/^{204}\text{Pb}$. Southern Ocean ferromanganese crust and nodule data (Abouchami and Goldstein, 1995; von Blanckenburg et al., 1996; Vlastelic et al., 2001; Fig. 1) provide evidence on the likely pre-anthropogenic composition of seawater in this region, which is dominantly influenced by continental weathering inputs that are represented here by the estimated average composition of the Upper Continental Crust (Garcon et al., 2013). Anthropogenic sources are represented by Tasmanian aerosols (Bollhofer and Rosman, 2000), recent sediments from the Derwent River, Tasmania (Townsend and Seen, 2012), and the modern day compositions of seawater from a South Atlantic profile (cruise D357, station 3, 36°S, 13°E; Paul et al., 2015a) (locations in Fig. 1). The uncleaned coral E from our cleaning experiment may also provide an indication of local anthropogenic Pb sources, although it was collected from a shallower depth (~1.2 km) than the deglacial corals. The dashed arrow points in the direction of those potential anthropogenic Pb sources. Water masses are labelled for the modern seawater data: AAIW = Antarctic Intermediate Water; NADW = North Atlantic Deep Water; CDW = Circumpolar Deep Water.

expected based on distribution coefficients of Pb in corals and likely deep ocean Pb concentrations (Section 1.3). However, much higher Pb concentrations in a few deglacial samples (Table 3), as well as in the cleaned corals from the cleaning experiment (Table 2), suggest that nano-scale phases could sometimes be important Pb carriers and may not always be completely removed by physical or chemical cleaning, as previously suggested by Adkins et al. (2004). Such phases could include seawater-derived Pb (e.g. organic particles, ferromanganese oxides; Adkins et al., 2004), but possibly also terrigenous grains (e.g. clays; Gutjahr et al., 2013). For the Tasmanian corals, while recognising that these measurements were made on separate subsamples, the lack of a relationship between Pb concentrations and ^{232}Th concentrations (Hines et al., 2015), which would be elevated by the incorporation of terrigenous particles, does not appear to support terrigenous particles as the controlling phase. Given that there is also no relationship between Pb isotopes and Pb concentrations in these corals, it appears more likely that the Pb in any nano-scale phases has also been derived from seawater. Although it is not clear how much Pb is contained within the aragonite matrix versus that carried in nano-scale accessory phases (e.g. oxides or organics), this scenario should not significantly impact on the ability of corals to record seawater Pb isotopic compositions. Nevertheless, future work should be carried out to evaluate the mechanisms and timescale over which such phases are formed and to better constrain distribution coefficients for Pb in deep-sea corals.

4.2. Deglacial evolution of Pb isotopes in the mid-depth Southern Ocean

4.2.1. Binary mixing of seawater Pb recorded in coral skeletons

The Pb isotope data from the deglacial corals overlap with the composition of Southern Ocean ferromanganese crusts and nodules (Abouchami and Goldstein, 1995; von Blanckenburg et al., 1996; Vlastelic et al., 2001) (Fig. 8) and clearly resolve binary mixing of two Pb sources in the mid-depth Southern Ocean south of Tasmania. The ultimate source of Pb to both the crusts and corals is predominantly from the weathering of continental rocks (e.g. typical values for the upper continental crust shown by black box in Fig. 8), with distinct signatures potentially supplied from different regions and transported and mixed by ocean currents. Although the plotted ferromanganese crust data are from a range of sectors and water depths of the Southern Ocean (Fig. 1), and predominantly from much deeper depths than the corals, they provide a first-order indication of the range of seawater Pb isotopic compositions that could potentially have influenced this location through time. In particular, there is excellent agreement between the deglacial coral data and the nearby ferromanganese crust SO-36/52KD (Fig. 6; von Blanckenburg et al., 1996), which was collected from south of Tasmania at a comparable water depth (1.7 km depth).

The deglacial coral data also record Pb isotopic variability on short timescales (Fig. 7), extending along a binary

mixing line to somewhat less radiogenic Pb isotopic compositions than the nearby crust SO-36/52KD (Fig. 6). The least radiogenic coral sample clearly lies outside the field of all Southern Ocean ferromanganese nodule data (Fig. 9a,b), and a couple of samples are outside the limits of those data when considering $^{207}\text{Pb}/^{204}\text{Pb}$ at a given $^{206}\text{Pb}/^{204}\text{Pb}$. Based on their isotopic compositions, we cannot rule out that the deglacial corals with the least radiogenic compositions may be seeing an anthropogenic Pb contaminant that has not been fully removed in these cases (Fig. 8), but we argue against this possibility for three reasons. First, the tightly constrained mixing lines in Pb-Pb space (Fig. 6) contrast with the wide variability in laboratory blank compositions (Section 3.1.3), suggesting that laboratory contamination would be unsuitable to explain the observed data. Second, the results of our cleaning experiment suggest that combined physical and chemical cleaning is very effective at removing surficial contaminants, even from a heavily contaminated coral (Fig. 5). Third, there is no indication of elevated Pb concentrations in the samples with the least radiogenic isotopic compositions (Table 3), which is contrary to expectations if they were recording the addition of recent anthropogenic Pb. We therefore consider that natural seawater-derived Pb controls the measured Pb isotopic composition of the deglacial coral samples. In that case, coral values that extend beyond the range recorded in ferromanganese crusts appear to indicate variability in Pb sources over short timescales that is hidden by temporal averaging in the crust and nodule data (e.g. Wilson et al., 2015a).

4.2.2. Advection sources of Pb

Since the majority of the coral samples record Pb isotopic compositions within the field of Southern Ocean ferromanganese crusts and nodules (Fig. 9a,b), water mass mixing may be the main control on the coral data. In general, the deeper depths of the Southern Ocean record more radiogenic Pb isotopic compositions (Abouchami and Goldstein, 1995; Vlastelic et al., 2001; van de Flierdt et al., 2006), raising the possibility that mixing between water masses at different depths could have influenced the Pb isotopic composition at Tasmania through time. However, it seems unlikely that the deep and bottom water masses of the Southern Ocean could have shoaled sufficiently to provide a significant contribution at the ~1.4–1.7 km depths of the corals. We therefore caution against a direct comparison with ferromanganese crust and nodule data from the deep basins. Considering that ~80% of the crust and nodule data were recovered from 3.0 to 5.5 km water depth, our following discussion necessarily focuses on the evidence from the relatively small number of crusts and nodules recovered from mid-depths of the Southern Ocean.

Given the strong eastward flow in the Antarctic Circumpolar Current, lateral advection may be important in supplying Pb to the Tasmanian corals from upstream. In that context, it is notable that mid-depth ferromanganese crusts from the Kerguelen Plateau (1.2–2.6 km water depths; Fig. 1) record a range of Pb isotopic variability that is comparable to that seen in the deglacial corals (when excluding

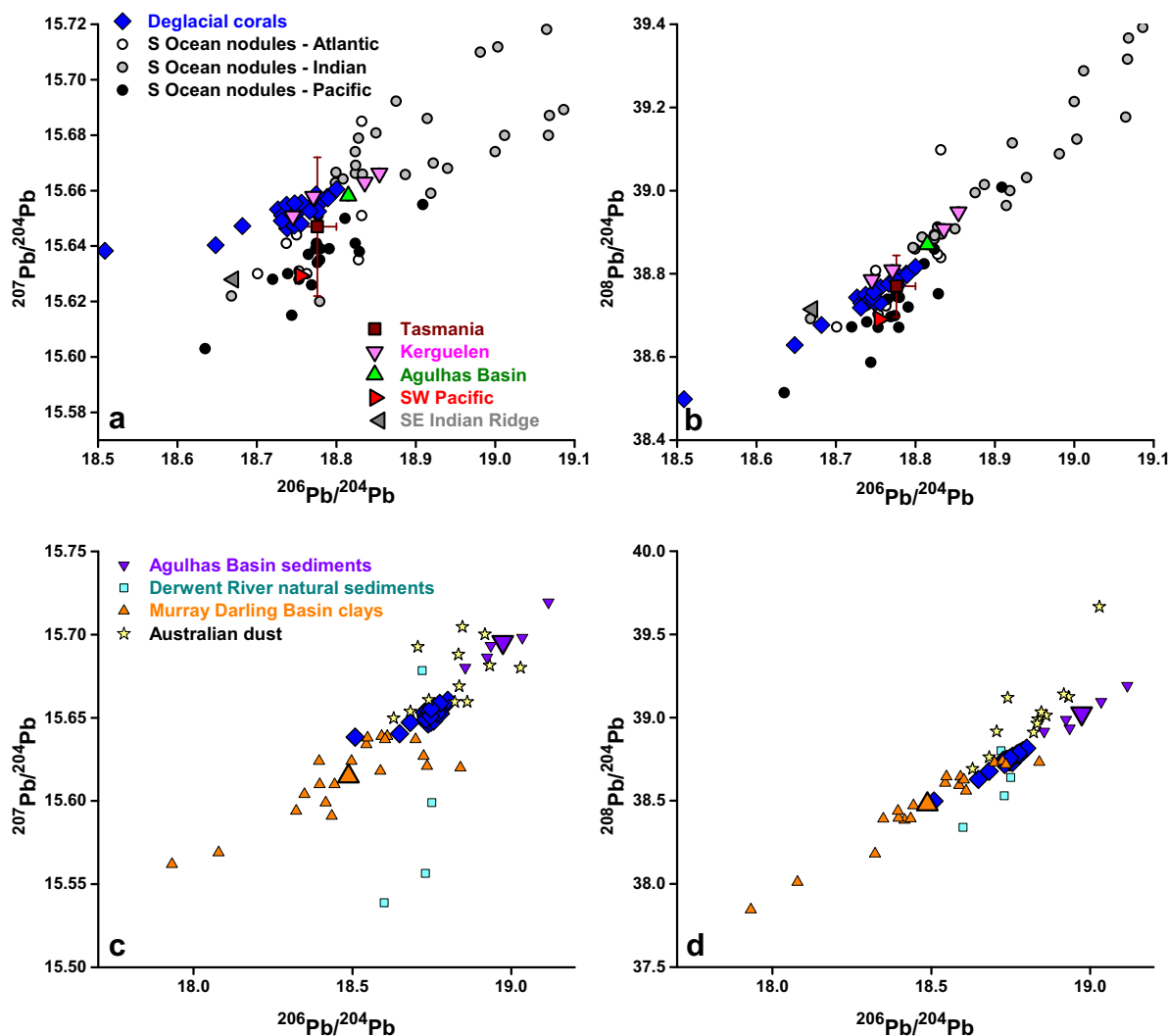


Fig. 9. Potential sources of natural Pb to the glacial and deglacial corals, assessed from (a,c) $^{207}\text{Pb}/^{204}\text{Pb}$ versus $^{206}\text{Pb}/^{204}\text{Pb}$, and (b,d) $^{208}\text{Pb}/^{204}\text{Pb}$ versus $^{206}\text{Pb}/^{204}\text{Pb}$. (a,b) Coral data compared to Southern Ocean ferromanganese crust and nodule data (Abouchami and Goldstein, 1995; von Blanckenburg et al., 1996; Vlastelic et al., 2001), distinguished by sector (Fig. 1). Particular samples are highlighted: Tasmanian sample SO-36/52KD (von Blanckenburg et al., 1996); Kerguelen samples DR8604, DR8605, DR8607 and DR8608 (Vlastelic et al., 2001); Agulhas Basin sample V29-D6 (Vlastelic et al., 2001); southwest Pacific sample SO-36/63KD (van de Flierdt et al., 2004a); and Southeast Indian Ridge sample E-PhC/54-6 (Vlastelic et al., 2001). Error bars are only shown for those highlighted samples and represent external reproducibility (2 s.d.); for data from Vlastelic et al. (2001) and van de Flierdt et al. (2004a) the uncertainties are comparable to symbol size. (c,d) Coral data compared to potential sedimentary input sources: detrital sediments from the northern Agulhas Basin (cores ODP 1088-1090; Noble et al., 2012) (large symbol represents the mean); pre-anthropogenic sediments from Derwent River, Tasmania (Townsend and Seen, 2012); Murray Darling Basin clays (de Deckker et al., 2010; de Deckker and Norman, 2010) (large symbol represents the mean); and chemically extracted fine fractions from Australian dust source areas (Vallelonga et al., 2010) (locations in Fig. 1). For simplicity, error bars are not shown in the lower panels, but the range of variability may be assessed from the fields of data.

the one outlying unradiogenic data point) (Fig. 9a,b). Since those crust data reflect some combination of temporal and spatial variations, they clearly indicate the potential for a resolvable level of Pb isotopic variability in the Antarctic Circumpolar Current upstream of Tasmania. Furthermore, the radiogenic Pb isotopic composition of nodule V29-D6 from the Agulhas Basin (~3.0 km depth; Fig. 1) also overlaps with the Kerguelen crust and Tasmanian coral array (Fig. 9a,b), which suggests that a radiogenic Pb isotope signal is being carried with North Atlantic Deep Water

(NADW) as it mixes eastwards within the CDW depth range (Abouchami and Goldstein, 1995; Vlastelic et al., 2001). While that ‘Atlantic’ signal could potentially have been generated within the South Atlantic basin and exported with NADW, detrital sediment input to the Atlantic sector of the Southern Ocean (and its subsequent dissolution or exchange with seawater) could also provide a Pb source within the Antarctic Circumpolar Current. In particular, detrital sediments from the northern Agulhas Basin sites 1088–1090 of ODP Leg 177 (Noble et al., 2012) appear

to represent a suitable radiogenic endmember for the coral array (Fig. 9c,d), which suggests that southern African sediment inputs may be responsible for generating this signal. Meanwhile, the southern sites 1093 and 1094 from that study record less radiogenic Pb isotopic compositions, potentially reflecting South American and/or Antarctic inputs (Noble et al., 2012), but while there is some overlap of those data with the coral array, those sediments do not reach sufficiently unradiogenic compositions to provide the unradiogenic endmember for all the coral samples.

Given the hydrographic setting of the corals near the boundary with Pacific water masses, the southwards advection of PDW might also be considered as a possible influence at Tasmania (Fig. 2b) and a potential source of unradiogenic Pb (Abouchami and Goldstein, 1995). Indeed, the most proximal mid-depth southwest Pacific ferromanganese crust SO-36/63KD (1.7 km water depth; Fig. 1) records distinctly unradiogenic values in its outer layer (e.g. $^{206}\text{Pb}/^{204}\text{Pb} = 18.75$; van de Flierdt et al., 2004a; Fig. 9a,b). However, in detail, data from SO-36/63KD (and also data from the Pacific sector of the Southern Ocean more generally) have too low a $^{207}\text{Pb}/^{204}\text{Pb}$ ratio (at a given $^{206}\text{Pb}/^{204}\text{Pb}$) for a PDW source to represent the unradiogenic endmember for the corals (Fig. 9a). Therefore, intervals with less radiogenic coral compositions cannot simply reflect an increased Pacific influence south of Tasmania.

To summarise, the above discussion demonstrates that (i) Pb isotopic variability in the Southern Ocean upstream of Tasmania is sufficient to explain the range of values seen in our coral data (with the exception of one outlying unradiogenic data point); and (ii) a radiogenic Pb isotope signal generated from continental inputs in the Atlantic sector and carried eastwards within the Antarctic Circumpolar Current represents a suitable radiogenic endmember for the mixing array.

4.2.3. Regional sources of Pb

In this section, we consider whether regional hydrothermal or sedimentary Pb sources could be influencing seawater and coral compositions more locally, and in particular address whether they could represent the unradiogenic Pb endmember for the binary mixing array.

Although volcanic ridges or islands could represent a candidate for unradiogenic Pb inputs, Pb in hydrothermal fluids is mostly removed near the vent (Chen et al., 1986; Noble et al., 2015). Therefore, while the Pb isotopic composition of some ferromanganese crusts and nodules implies a local contribution of hydrothermal sources (Abouchami and Goldstein, 1995; Vlastelic et al., 2001; van de Flierdt et al., 2004b), such inputs have generally been considered to be negligible for the deep ocean Pb budget. Here, we rule out any significant influence from the Kerguelen and Heard Islands, which are upstream in the Antarctic Circumpolar Current flow path, because the Pb isotopic composition of those ocean island basalts is not seen in Kerguelen ferromanganese crusts (Abouchami and Goldstein, 1995), and would in any case not represent a suitable endmember (i.e., $^{208}\text{Pb}/^{204}\text{Pb}$ is too high at a given $^{206}\text{Pb}/^{204}\text{Pb}$) (Iwamori et al., 2010). Basalts from the more proximal

Southeast Indian Ridge (Iwamori et al., 2010) appear to have influenced the composition of ferromanganese crust E-PhC/54-6 (3.42 km depth; Fig. 1) collected from near the ridge crest (Abouchami and Goldstein, 1995; Vlastelic et al., 2001) (Fig. 9a,b). However, in detail, both those basalts and crust E-PhC/54-6 have $^{207}\text{Pb}/^{204}\text{Pb}$ ratios that are too low at a given $^{206}\text{Pb}/^{204}\text{Pb}$ to fall along an extension of the coral array (Fig. 9a), suggesting that this source may also be ruled out. By the same reasoning, basalts from the Pacific-Antarctic Ridge (Hamelin et al., 2011) are also an unsuitable source.

Given the short ocean residence time of Pb, it is reasonable to consider whether local inputs from Tasmania could provide a Pb source to the mid-depth ocean. Unfortunately, riverine evidence from Tasmania is limited, but the Pb isotopic compositions of pre-anthropogenic river sediments from the Derwent and Huon rivers of Tasmania (Townsend and Seen, 2012) (Fig. 9c,d) are not suitable endmembers for the deglacial coral mixing line. Similarly, considering Tasmanian bedrock lithologies, neither the Jurassic dolerite that comprises eastern Tasmania (Allegre et al., 1982; Hergt et al., 1989), nor the Tertiary plume-related basalts that form seamounts off its southern coast (Ewart et al., 1988; Lanyon et al., 1993), have compositions that overlap with the coral array. We therefore argue against a local control on the coral record, although more data on the composition of Tasmanian inputs (particularly from the Proterozoic basement rocks of western Tasmania) would be useful before this possibility could be completely ruled out.

Considering more regional sources, the Pb isotopic composition of potential dust source areas in Australia (Fig. 9c, d; Vallelonga et al., 2010; see Fig. 1 for sampling locations), combined with evidence for a dust plume originating in this region (Mahowald et al., 2011), suggests that some contribution from Australian dust input is possible. However, those data are insufficiently unradiogenic for dust to represent the unradiogenic endmember (Fig. 9c,d). In contrast, the compositions of riverine clays from the Murray Darling Basin (de Deckker et al., 2010; de Deckker and Norman, 2010), which is the major river system draining south and southeast Australia (Fig. 1), plot close to the most unradiogenic coral data along an extension of the mixing array (Fig. 9c,d). Despite the modest discharge and sediment yields from the Darling River today (Milliman and Meade, 1983), it appears that such Australian riverine inputs could represent the unradiogenic endmember, and at times may have contributed significantly to the ocean Pb budget in this region. Such local surface Pb inputs could be transferred by riverine input and vertical particle exchange (Henderson and Maier-Reimer, 2002), or through boundary exchange processes between margin sediments and seawater (Vlastelic et al., 2001; Wilson et al., 2015a; Chen et al., 2016), thereby allowing this riverine signature to reach the mid-depths of the Southern Ocean. The transfer of such a signature from southern Australia to south of Tasmania (~1500 km) appears feasible since both data (Abouchami and Goldstein, 1995; Vlastelic et al., 2001) and models (Henderson and Maier-Reimer, 2002) indicate Pb isotope mixing domains on length scales of thousands

of kilometres in the deep ocean, and given also that these distances could be extended by rapid advection within the Antarctic Circumpolar Current.

4.2.4. Paleoclimate implications of glacial-interglacial stability and millennial variability

Our deglacial coral Pb isotope record, based on samples from ~1.4–1.7 km water depths and covering the interval ~12–40 ka BP, records millennial timescale variability but no glacial-interglacial trend (Fig. 7). In some cases, Pb isotope changes through time could arise due to changes in weathering mechanism or intensity in the source regions of Pb supplied to the oceans, leading to the preferential release of radiogenic Pb from radiation-damaged sites or radiogenic accessory minerals in the period following glacial erosion (Erel et al., 1994; Harlavan and Erel, 2002). However, while that interpretation may be relevant to records from the North Atlantic close to the glaciated margins of Greenland and Laurentia (Foster and Vance, 2006; Gutjahr et al., 2009; Crocket et al., 2012), such a control appears unlikely in the present setting south of Tasmania. Both the high frequency variability and the lack of a clear glacial-interglacial signal in our deep-sea coral record (Fig. 10c) are quite distinct from those North Atlantic Pb isotope records, making it hard to invoke a glacial weathering control. Instead, to a first order, our record indicates a general stability of the Pb sources to the ocean through time, as previously observed in glacial-interglacial ferromanganese crust records from the Pacific Ocean (Abouchami et al., 1997) and Atlantic Ocean (Claude-Ivanaj et al., 2001). Therefore, we focus on mixing between two fixed and isotopically distinct Pb sources as the major control on millennial variability in the coral record. In that scenario, the simplest explanation involves mixing between radiogenic Pb derived from upstream in the Antarctic Circumpolar Current (Atlantic-Indian sector) and regionally-sourced unradiogenic riverine Pb inputs from Australia. Temporal variability could then be due to changes in Pb inputs in the Atlantic sector, changes in their transport to Tasmania, or changes in the regional Australian Pb inputs.

In order to decipher the likely controls on our new Pb isotope record, we first consider its relationship to other tracer reconstructions from the deglacial Southern Ocean (Fig. 10). Although there are no published deglacial Nd isotope records from fully within the Southern Ocean, a number of studies have inferred its temporal evolution from locations in the Atlantic, Indian and Pacific basins that are ventilated predominantly by southern-sourced water masses, at both intermediate and deep depths (e.g. Piotrowski et al., 2012; Noble et al., 2013; Wilson et al., 2015b; Hu et al., 2016). Those reconstructions are dominated by a glacial-interglacial shift of ~1.5–3 ϵ_{Nd} units (Fig. 10e), which has generally been interpreted in terms of a reduced influence of Atlantic (NADW) versus Pacific (PDW) derived water masses in the Southern Ocean during the last glacial period. Since our Pb isotope record (Fig. 10c) lacks a glacial-interglacial trend and instead shows high frequency variations, these two tracers appear to be decoupled in this location. Given the shorter deep

ocean residence time of Pb than Nd, it is perhaps unsurprising that the Pb isotope record is not responding in the same way as Nd isotopes to global or basin scale circulation changes. In a simple global model, Henderson and Maier-Reimer (2002) inferred particularly short deep ocean residence times for Pb in the Southern Ocean (~10–30 years), which are at least an order of magnitude shorter than global estimates of deep ocean Nd residence times (Siddall et al., 2008; Rempfer et al., 2011). Therefore, if water mass mixing is influencing the deglacial Pb isotope evolution, then it must be recording mixing over shorter time and length scales than the intra-basin mixing recorded by Nd isotopes. Alternatively, due to its shorter residence time, the Pb isotope record may be responding to variations in southern African or Australian continental inputs, without these significantly influencing the Nd isotope budget of the Southern Ocean. In either case, the distinct behaviour of Pb isotopes through time appears to provide some support that those Nd isotope records are indeed reflecting more global changes.

There is also no simple relationship between our new Pb isotope record and radiocarbon reconstructions made on the same set of Tasmanian corals (Hines et al., 2015) (Fig. 10d), which clearly reflects the different processes controlling these tracers. Whereas radiocarbon signatures are set by atmospheric exchange in water mass source regions and subsequent ventilation timescales, leading to interpretations of deglacial variability in terms of surface ocean frontal shifts (Hines et al., 2015), Pb isotopes in this location are expected to record an integrated signal of Pb supplied to the Southern Ocean from water masses and/or sedimentary sources and would not be simply reset by exposure at the high latitude ocean surface.

While there is no clear glacial-interglacial shift in the coral-based Pb isotope record, the indication of millennial timescale variability is an interesting feature, which may possibly be related to Heinrich stadials in the North Atlantic and their corresponding Antarctic warm events in the Southern Ocean (pink bars in Fig. 10). However, given the modest sampling resolution of the record, a shift towards more radiogenic Pb isotopic compositions at the start of warm intervals in the Southern Ocean is only clearly resolved for Heinrich Stadial 1. Such a shift in Pb isotopes could be caused by a number of mechanisms, reflecting circulation or climate change in the Southern Ocean. We suggest that the simplest interpretation would involve an increase in lateral transport of the radiogenic Pb isotope signature carried from the Atlantic sector and/or Agulhas Basin via Kerguelen Plateau (Abouchami and Goldstein, 1995; Vlastelic et al., 2001), thereby reducing the relative contribution of unradiogenic Australian Pb inputs at these times. Intriguingly, recent sedimentological evidence for enhanced flow speed in the northern branch of the Antarctic Circumpolar Current during Antarctic warm events (Lamy et al., 2015) (Fig. 10b), potentially tied to warmer temperatures and equatorward-shifted southern westerly winds, appears to support this idea. We therefore suggest that Pb isotopes may be responding to mixing dynamics within the Antarctic Circumpolar Current, but

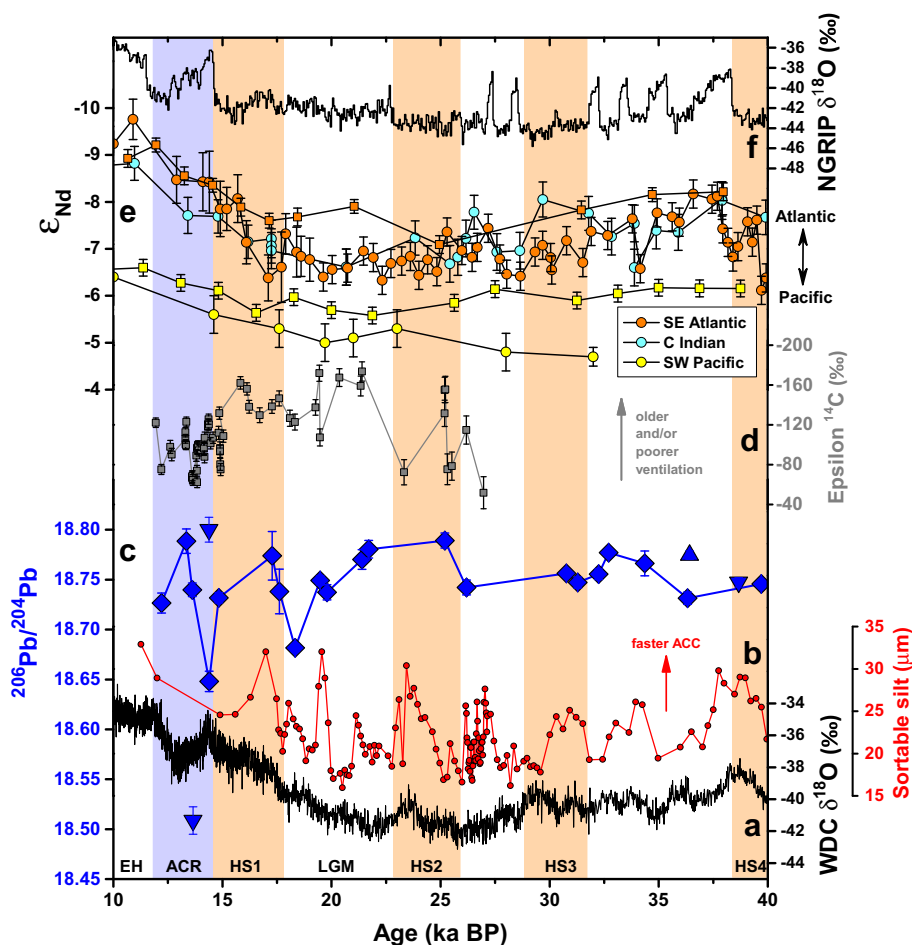


Fig. 10. Late glacial and deglacial coral Pb isotope record compared to records of climatic and oceanographic variability. (a) Antarctic ice core $\delta^{18}\text{O}$ temperature proxy record from WAIS Divide Core (WDC; Buizert et al., 2015). (b) Sortable silt record from sediment core MD07-3128 (1.03 km water depth) within the northern Antarctic Circumpolar Current (Lamy et al., 2015). (c) Tasmanian coral Pb isotope record ($^{206}\text{Pb}/^{204}\text{Pb}$; other ratios have a similar pattern), as in Fig. 7 but with error bars showing estimated external reproducibility calculated as 3 times internal precision (see Fig. 4d). (d) Tasmanian coral radiocarbon record based on samples from 1.43–1.75 km water depth, plotted as Epsilon ^{14}C units (Hines et al., 2015). (e) Neodymium isotope reconstructions from locations influenced by southern-sourced water masses. Deep ocean records (circles) from: southeast Atlantic Ocean (~ 5.0 km; TNO57-21; Piotrowski et al., 2008, 2012); central Indian Ocean (~ 3.8 km; SK129-CR2; Wilson et al., 2015b); southwest Pacific Ocean (~ 4.2 km; CHAT 5K; Noble et al., 2013). Mid-depth records (squares) from southeast Atlantic Ocean (~ 1.4 km; ODP 1087; Hu et al., 2016); southwest Pacific Ocean (~ 1.3 km; Y9; Hu et al., 2016). (f) Greenland ice core $\delta^{18}\text{O}$ temperature proxy record from NGRIP (NGRIP, 2004). Locations of sediment core records are shown in Fig. 1. Uncertainties in coral ages are smaller than symbol sizes. Time intervals are labelled along the x axis: ACR = Antarctic Cold Reversal; EH = Early Holocene; HS = Heinrich Stadial; LGM = Last Glacial Maximum. ACC = Antarctic Circumpolar Current.

additional records from other locations, and higher resolution evidence during key intervals, would be necessary in order to confirm such a hypothesis.

Finally, we note that the most extreme excursions to unradiogenic Pb isotope compositions were recorded during the Last Glacial Maximum and Antarctic Cold Reversal (Fig. 10c). If the Antarctic Circumpolar Current was weaker at these times (Fig. 10b), the reduction in transport from upstream may have led to a greater dominance of local unradiogenic riverine inputs from the Murray Darling Basin, while changing riverine input fluxes tied to Australian climate could represent a potential additional control. Enhanced precipitation over south and southeast Australia during the deglaciation, potentially related to enhanced La Nina conditions and/or

extended southern westerly winds (Vandergoes and Fitzsimons, 2003; Petherick et al., 2013), is indicated by records of enhanced fluvial activity (and high variability) in the Murray Darling Basin. For example, there were high flow conditions in the Murray Darling Basin from around 20–12 ka BP (Page et al., 1996, 2009), and increased fluvial-derived illite is recorded in the marine sediments of Murray Canyon at ~ 13.5 ka BP during the Antarctic Cold Reversal (Gingele et al., 2007). The Tasmanian coral Pb isotope record may have responded to such input changes, thereby providing evidence on such regional climate shifts, but fully deciphering the roles of changing inputs versus current transport will require more extensive multi-proxy tracer reconstructions within the Southern Ocean.

5. CONCLUSIONS

We have developed a procedure to obtain robust Pb isotopic composition data (including the minor ^{204}Pb isotope) on ~ 500 mg of fossil coral aragonite, typically containing ~ 5 ng of Pb. Our method includes physical and chemical cleaning, digestion, a 2-step anion exchange chemistry procedure, and analysis by TIMS using a ^{207}Pb – ^{204}Pb double spike. By using a $10^{12} \Omega$ resistor to measure the ^{204}Pb beam, we obtain a significant improvement in both internal precision and long term external reproducibility, thereby aiding application to small sample sizes. For example, measurements on a 2 ng NIST-SRM-981 Pb standard indicate an internal precision on $^{208}\text{Pb}/^{204}\text{Pb}$ of ~ 230 ppm and external reproducibility of ~ 550 ppm.

Coral cleaning experiments demonstrate that physical and chemical cleaning are necessary to remove recent anthropogenic Pb contaminants and to recover natural Pb isotopic compositions from deep-sea corals. In that case, the good agreement with the compositions of ferromanganese crusts and nodules suggests that deep-sea coral aragonite may provide a reliable archive of dissolved seawater Pb isotopic composition for the pre-anthropogenic oceans. In addition, the precision and reproducibility of our measurements, even those made on a few nanograms of Pb, has a good resolving power in comparison to the spatial and temporal variability of Pb isotopes recorded in the oceans (e.g. Abouchami and Goldstein, 1995; Vlastelic et al., 2001; Wilson et al., 2015a), and particularly in the North Atlantic (e.g. Foster and Vance, 2006; Gutjahr et al., 2009).

In order to start exploiting the potential of this approach, we generated a Pb isotope time series from a collection of late glacial and deglacial deep-sea corals from the mid-depth Southern Ocean south of Tasmania. Those data record binary mixing in Pb isotope space, which can be explained by mixing between a radiogenic endmember transported from upstream within the Antarctic Circumpolar Current and an unradiogenic endmember, potentially supplied locally from Australia. Over glacial-interglacial timescales, the temporal constancy of Pb sources to the corals contrasts with glacial-interglacial Nd isotope shifts in Southern Ocean water masses, highlighting the ability of Pb and Nd isotopes to provide complementary paleoceanographic information in this region. In addition, Pb isotope variability on millennial timescales appears to record dynamic changes within the Antarctic Circumpolar Current, but potentially also climatically-controlled changes in continental inputs.

For a wider application of Pb isotopes in the deep-sea coral archive, and particularly for high resolution reconstructions, future studies will need to further investigate the mechanisms and timescale of Pb incorporation into coral skeletons, the possible role of minor accessory phases in controlling Pb concentrations, and the potential influence of post-mortem addition of anthropogenic Pb. In addition, higher resolution records and wider geographical coverage would advance our understanding of Pb isotopes as a tracer in deep-sea corals and improve paleoceanographic interpretations. Considering the improved sensitiv-

ity of the new generation of MC-ICP-MS instruments, and the potential for increased precision offered by 10^{12} or $10^{13} \Omega$ resistors, such a prospect now appears feasible.

ACKNOWLEDGEMENTS

This study was supported by Leverhulme Trust grant RPG-398 to TvdF, and NERC grant NE/N001141/1 to TvdF and DJW. We are very grateful to Sophia Hines for assistance with sampling from the Caltech coral collection and for providing published and unpublished U–Th ages; Luke Bridgestock for providing some of the NIST-SRM-981 standard data measured on the $10^{11} \Omega$ resistor; Kirsty Crocket for supplying the coral powder used to prepare the in-house coral Pb standard; and Maxence Paul for establishing the double spike TIMS method at Imperial and for his initial efforts during installation of the $10^{12} \Omega$ resistor. Katharina Kreissig and Barry Coles provided invaluable maintenance of the MAGIC clean labs and mass spectrometers. We further appreciate careful and thoughtful reviews from Wafa Abouchami, Ed Boyle and Marcus Gutjahr, and editorial handling by Claudine Stirling.

APPENDIX A. SUPPLEMENTARY DATA

Supplementary data associated with this article can be found, in the online version, at <http://dx.doi.org/10.1016/j.gca.2017.01.052>.

REFERENCES

- Abouchami W. and Goldstein S. L. (1995) A lead isotopic study of Circum-Antarctic manganese nodules. *Geochim. Cosmochim. Acta* **59**, 1809–1820.
- Abouchami W., Goldstein S. L., Galer S. J. G., Eisenhauer A. and Mangini A. (1997) Secular changes of lead and neodymium in central Pacific seawater recorded by a Fe–Mn crust. *Geochim. Cosmochim. Acta* **61**, 3957–3974.
- Adkins J. F., Henderson G. M., Wang S. L., O’Shea S. and Mokadem F. (2004) Growth rates of the deep-sea scleractinia *Desmophyllum cristagalli* and *Enallopsammia rostrata*. *Earth Planet. Sci. Lett.* **227**, 481–490.
- Allegre C. J., Dupre B., Richard P., Rousseau D. and Brooks C. (1982) Sub-continental versus sub-oceanic mantle, II. Nd–Sr–Pb isotopic comparison of continental tholeiites with mid-ocean ridge tholeiites, and the structure of the continental lithosphere. *Earth Planet. Sci. Lett.* **57**, 25–34.
- Alleman L. Y., Veron A. J., Church T. M., Flegal A. R. and Hamelin B. (1999) Invasion of the abyssal North Atlantic by modern anthropogenic lead. *Geophys. Res. Lett.* **26**, 1477–1480.
- Arsouze T., Dutay J. C., Lacan F. and Jeandel C. (2009) Reconstructing the Nd oceanic cycle using a coupled dynamical – biogeochemical model. *Biogeosciences* **6**, 2829–2846.
- Basak C., Martin E. E. and Kamenov G. D. (2011) Seawater Pb isotopes extracted from Cenozoic marine sediments. *Chem. Geol.* **286**, 94–108.
- Bizzarro M., Baker J. A., Haack H., Ulfbeck D. and Rosing M. (2003) Early history of Earth’s crust–mantle system inferred from hafnium isotopes in chondrites. *Nature* **421**, 931–933.
- Bollhofer A. and Rosman K. J. R. (2000) Isotopic source signatures for atmospheric lead: the Southern Hemisphere. *Geochim. Cosmochim. Acta* **64**, 3251–3262.
- Bostock H. C., Sutton P. J., Williams M. J. M. and Opdyke B. N. (2013) Reviewing the circulation and mixing of Antarctic Intermediate Water in the South Pacific using evidence from

- geochemical tracers and Argo float trajectories. *Deep-Sea Res. Part I-Oceanogr. Res. Pap.* **73**, 84–98.
- Boyle E. A., Lee J. M., Echevoyen Y., Noble A., Moos S., Carrasco G., Zhao N., Kayser R., Zhang J., Gamo T., Obata H. and Norisuye K. (2014) Anthropogenic lead emission in the ocean: the evolving global experiment. *Oceanography* **27**, 69–75.
- Buizert C., Adrian B., Ahn J., Albert M., Alley R. B., Baggenstos D., Bauska T. K., Bay R. C., Bencivengo B. B., Bentley C. R., Brook E. J., Chellman N. J., Clow G. D., Cole-Dai J., Conway H., Cravens E., Cuffey K. M., Dunbar N. W., Edwards J. S., Fegyveresi J. M., Ferris D. G., Fitzpatrick J. J., Fudge T. J., Gibson C. J., Gkinis V., Goetz J. J., Gregory S., Hargreaves G. M., Iverson N., Johnson J. A., Jones T. R., Kalk M. L., Kippenhan M. J., Koffman B. G., Kreutz K., Kuhl T. W., Lebar D. A., Lee J. E., Marcott S. A., Markle B. R., Maselli O. J., McConnell J. R., McGwire K. C., Mitchell L. E., Mortensen N. B., Neff P. D., Nishiizumi K., Nunn R. M., Orsi A. J., Pasteris D. R., Pedro J. B., Pettit E. C., Price P. B., Priscu J. C., Rhodes R. H., Rosen J. L., Schauer A. J., Schoenemann S. W., Sendelbach P. J., Severinghaus J. P., Shturmakov A. J., Sigl M., Slawny K. R., Souney J. M., Sowers T. A., Spencer M. K., Steig E. J., Taylor K. C., Twickler M. S., Vaughn B. H., Voigt D. E., Waddington E. D., Welten K. C., Wendricks A. W., White J. W. C., Winstrup M., Wong G. J., Woodruff T. E. and Members W. D. P. (2015) Precise inter-polar phasing of abrupt climate change during the last ice age. *Nature* **520**, 661–665.
- Chen J. H., Wasserburg G. J., Vondamm K. L. and Edmond J. M. (1986) The U-Th-Pb systematics in hot springs on the East Pacific Rise at 21 N and Guaymas Basin. *Geochim. Cosmochim. Acta* **50**, 2467–2479.
- Chen T. Y., Robinson L. F., Burke A., Southon J., Spooner P., Morris P. J. and Ng H. C. (2015) Synchronous centennial abrupt events in the ocean and atmosphere during the last deglaciation. *Science* **349**, 1537–1541.
- Chen M., Boyle E. A., Lee J.-M., Nurhati I., Zurbrück C., Switzer A. D. and Carrasco G. (2016) Lead isotope exchange between dissolved and fluvial particulate matter: a laboratory study from the Johor River estuary. *Philos. Trans. R. Soc. A Math. Phys. Eng. Sci.* **374**, 20160054. <http://dx.doi.org/10.1098/rsta.2016.0054>.
- Cheng H., Adkins J., Edwards R. L. and Boyle E. A. (2000) U-Th dating of deep-sea corals. *Geochim. Cosmochim. Acta* **64**, 2401–2416.
- Claude-Ivanaj C., Hofmann A. W., Vlastelic I. and Koschinsky A. (2001) Recording changes in ENADW composition over the last 340 ka using high-precision lead isotopes in a Fe–Mn crust. *Earth Planet. Sci. Lett.* **188**, 73–89.
- Cochran J. K., McKibbin-Vaughan T., Dornblaser M. M., Hirschberg D., Livingston H. D. and Buesseler K. O. (1990) ²¹⁰Pb scavenging in the North Atlantic and North Pacific Oceans. *Earth Planet. Sci. Lett.* **97**, 332–352.
- Colin C., Frank N., Copard K. and Douville E. (2010) Neodymium isotopic composition of deep-sea corals from the NE Atlantic: implications for past hydrological changes during the Holocene. *Quat. Sci. Rev.* **29**, 2509–2517.
- Crocket K. C., Vance D., Foster G. L., Richards D. A. and Tranter M. (2012) Continental weathering fluxes during the last glacial/interglacial cycle: insights from the marine sedimentary Pb isotope record at Orphan Knoll, NW Atlantic. *Quat. Sci. Rev.* **38**, 89–99.
- Crocket K. C., Lambelet M., van de Flierdt T., Rehkamper M. and Robinson L. F. (2014) Measurement of fossil deep-sea coral Nd isotopic compositions and concentrations by TIMS as NdO⁺, with evaluation of cleaning protocols. *Chem. Geol.* **374–375**, 128–140.
- de Deckker P. and Norman M. D. (2010) Re-evaluation of the composition of sediments from the Murray Darling Basin of Australia as a Potential Source Area for airborne dust to EPICA Dome C in Antarctica. Reply to Comment on “Lead isotopic evidence for an Australian source of aeolian dust to Antarctica at times over the last 170,000 years” by P. De Deckker, M. Norman, I.D. Goodwin, A. Wain and F.X. Gingele. *Palaeogeography, Palaeoclimatology, Palaeoecology* **285** (2010) 205–223. *Paleogeogr. Paleoclimatol. Paleoecol.* **298**, 437–442.
- de Deckker P., Norman M., Goodwin I. D., Wain A. and Gingele F. X. (2010) Lead isotopic evidence for an Australian source of aeolian dust to Antarctica at times over the last 170,000 years. *Paleogeogr. Paleoclimatol. Paleoecol.* **285**, 205–223.
- Echevoyen Y., Boyle E. A., Lee J. M., Gamo T., Obata H. and Norisuye K. (2014) Recent distribution of lead in the Indian Ocean reflects the impact of regional emissions. *Proc. Natl. Acad. Sci. USA* **111**, 15328–15331.
- Erel Y. G., Harlavan Y. and Blum J. D. (1994) Lead isotope systematics of granitoid weathering. *Geochim. Cosmochim. Acta* **58**, 5299–5306.
- Ewart A., Chapell B. W. and Menzies M. A. (1988) An overview of the geochemical and isotopic characteristics of the eastern Australian Cainozoic volcanic provinces. *J. Petrol. Spec. Lithos. Issue*, 225–273.
- Flegal A. R., Maring H. and Niemeyer S. (1993) Anthropogenic lead in Antarctic sea water. *Nature* **365**, 242–244.
- Foster G. L. and Vance D. (2006) Negligible glacial-interglacial variation in continental chemical weathering rates. *Nature* **444**, 918–921.
- Frank M. (2002) Radiogenic isotopes: tracers of past ocean circulation and erosional input. *Rev. Geophys.* **40**. <http://dx.doi.org/10.1029/2000rg000094>.
- Frank M. and O’Nions R. K. (1998) Sources of Pb for Indian Ocean ferromanganese crusts: a record of Himalayan erosion? *Earth Planet. Sci. Lett.* **158**, 121–130.
- Galer S. J. G. (1999) Optimal double and triple spiking for high precision lead isotopic measurement. *Chem. Geol.* **157**, 255–274.
- Galer S. J. G. and Abouchami W. (1998) Practical application of lead triple spiking for correction of instrumental mass discrimination. *Mineral. Mag.* **62A**, 491–492.
- Garcia, H.E., Locarnini, R.A., Boyer, T.P., Antonov, J.I., Baranova, O.K., Zweng, W.M., Reagan, J.R., Johnson, D.R., 2014. World Ocean Atlas 2013, Volume 3: Dissolved Oxygen, Apparent Oxygen Utilization, and Oxygen Saturation. In NOAA Atlas NESDIS 75 (ed., Levitus, S.).
- Garçon M., Chauvel C., France-Lanord C., Limonta M. and Garzanti E. (2013) Removing the “heavy mineral effect” to obtain a new Pb isotopic value for the upper crust. *Geochem. Geophys. Geosyst.* **14**, 3324–3333.
- Gingele F., De Deckker P. and Norman M. (2007) Late Pleistocene and Holocene climate of SE Australia reconstructed from dust and river loads deposited offshore the River Murray Mouth. *Earth Planet. Sci. Lett.* **255**, 257–272.
- Goldstein S. L. and Hemming S. R. (2003) Long-lived isotopic tracers in oceanography, paleoceanography and ice sheet dynamics. In *The Oceans and Marine Geochemistry* (ed. H. Elderfield). Elsevier-Pergamon, Oxford, pp. 453–489.
- Gutjahr M., Frank M., Halliday A. N. and Keigwin L. D. (2009) Retreat of the Laurentide ice sheet tracked by the isotopic composition of Pb in western North Atlantic seawater during termination 1. *Earth Planet. Sci. Lett.* **286**, 546–555.
- Gutjahr M., Vance D., Hoffmann D. L., Hillenbrand C. D., Foster G. L., Rae J. W. B. and Kuhn G. (2013) Structural limitations in deriving accurate U-series ages from calcitic cold-water

- corals contrast with robust coral radiocarbon and Mg/Ca systematics. *Chem. Geol.* **355**, 69–87.
- Hamelin B., Manhès G., Albarede F. and Allègre C. J. (1985) Precise lead isotope measurements by the double spike technique: a reconsideration. *Geochim. Cosmochim. Acta* **49**, 173–182.
- Hamelin C., Dosso L., Hanan B. B., Moreira M., Kositsky A. P. and Thomas M. Y. (2011) Geochemical portrait of the Pacific Ridge: new isotopic data and statistical techniques. *Earth Planet. Sci. Lett.* **302**, 154–162.
- Harlavan Y. and Erel Y. (2002) The release of Pb and REE from granitoids by the dissolution of accessory phases. *Geochim. Cosmochim. Acta* **66**, 837–848.
- Henderson G. M. and Maier-Reimer E. (2002) Advection and removal of ^{210}Pb and stable Pb isotopes in the oceans: a general circulation model study. *Geochim. Cosmochim. Acta* **66**, 257–272.
- Hergt J. M., Chappell B. W., McCulloch M. T., McDougall I. and Chivas A. R. (1989) Geochemical and isotopic constraints on the origin of the Jurassic dolerites of Tasmania. *J. Petrol.* **30**, 841–883.
- Hines S. K. V., Southon J. R. and Adkins J. F. (2015) A high-resolution record of Southern Ocean intermediate water radiocarbon over the past 30,000 years. *Earth Planet. Sci. Lett.* **432**, 46–58.
- Hu R., Noble T. L., Piotrowski A. M., McCave I. N., Bostock H. C. and Neil H. L. (2016) Neodymium isotopic evidence for linked changes in Southeast Atlantic and Southwest Pacific circulation over the last 200 kyr. *Earth Planet. Sci. Lett.* **455**, 106–114.
- Iwamori H., Albarede F. and Nakamura H. (2010) Global structure of mantle isotopic heterogeneity and its implications for mantle differentiation and convection. *Earth Planet. Sci. Lett.* **299**, 339–351.
- John S. G. and Adkins J. F. (2010) Analysis of dissolved iron isotopes in seawater. *Mar. Chem.* **119**, 65–76.
- Kelly A. E., Reuer M. K., Goodkin N. F. and Boyle E. A. (2009) Lead concentrations and isotopes in corals and water near Bermuda, 1780–2000. *Earth Planet. Sci. Lett.* **283**, 93–100.
- Klaver M., Smeets R. J., Koornneef J. M., Davies G. R. and Vroon P. Z. (2016) Pb isotope analysis of ng size samples by TIMS equipped with a 10^{13} ohm resistor using a ^{207}Pb – ^{204}Pb double spike. *J. Anal. Atm. Spectrom.* **31**, 171–178.
- Koornneef J. M., Bouman C., Schwieters J. B. and Davies G. R. (2014) Measurement of small ion beams by thermal ionisation mass spectrometry using new 10^{13} Ω resistors. *Anal. Chim. Acta* **819**, 49–55.
- Lamy F., Arz H. W., Kilian R., Lange C. B., Lembke-Jene L., Wengler M., Kaiser J., Baeza-Urrea O., Hall I. R., Harada N. and Tiedemann R. (2015) Glacial reduction and millennial-scale variations in Drake Passage throughflow. *Proc. Natl. Acad. Sci. USA* **112**, 13496–13501.
- Lanyon R., Varne R. and Crawford A. J. (1993) Tasmanian Tertiary basalts, the Balleny plume, and opening of the Tasman Sea (southwest Pacific Ocean). *Geology* **21**, 555–558.
- Lee J. M., Boyle E. A., Nurhati I. S., Pfeiffer M., Meltzner A. J. and Suwargadi B. (2014) Coral-based history of lead and lead isotopes of the surface Indian Ocean since the mid-20th century. *Earth Planet. Sci. Lett.* **398**, 37–47.
- Lee J. M., Boyle E. A., Gamo T., Obata H., Norisuye K. and Echevoy Y. (2015) Impact of anthropogenic Pb and ocean circulation on the recent distribution of Pb isotopes in the Indian Ocean. *Geochim. Cosmochim. Acta* **170**, 126–144.
- Lee J. M., Eltgroth S. F., Boyle E. A. and Adkins J. F. (2017) The transfer of bomb radiocarbon and anthropogenic lead to the deep North Atlantic Ocean observed from a deep sea coral. *Earth Planet. Sci. Lett.* **458**, 223–232.
- Lomitschka M. and Mangini A. (1999) Precise Th/U-dating of small and heavily coated samples of deep sea corals. *Earth Planet. Sci. Lett.* **170**, 391–401.
- Lugmair G. W. and Galer S. J. G. (1992) Age and isotopic relationships among the angrites Lewis Cliff 86010 and Angra dos Reis. *Geochim. Cosmochim. Acta* **56**, 1673–1694.
- Macdonald A. M., Mecking S., Robbins P. E., Toole J. M., Johnson G. C., Talley L., Cook M. and Wijffels S. E. (2009) The WOCE-era 3-D Pacific Ocean circulation and heat budget. *Prog. Oceanogr.* **82**, 281–325.
- Mahowald N., Albani S., Engelstaedter S., Winckler G. and Goman M. (2011) Model insight into glacial-interglacial paleodust records. *Quat. Sci. Rev.* **30**, 832–854.
- Milliman J. D. and Meade R. H. (1983) World-wide delivery of river sediment to the oceans. *J. Geol.* **91**, 1–21.
- NGRIP (2004) High-resolution record of Northern Hemisphere climate extending into the last interglacial period. *Nature* **431**, 147–151.
- Noble T. L., Piotrowski A. M., Robinson L. F., McManus J. F., Hillenbrand C. D. and Bory A. J. M. (2012) Greater supply of Patagonian-sourced detritus and transport by the ACC to the Atlantic sector of the Southern Ocean during the last glacial period. *Earth Planet. Sci. Lett.* **317**, 374–385.
- Noble T. L., Piotrowski A. M. and McCave I. N. (2013) Neodymium isotopic composition of intermediate and deep waters in the glacial southwest Pacific. *Earth Planet. Sci. Lett.* **384**, 27–36.
- Noble A. E., Echevoyen-Sanz Y., Boyle E. A., Ohnemus D. C., Lam P. J., Kayser R., Reuer M., Wu J. F. and Smethie W. (2015) Dynamic variability of dissolved Pb and Pb isotope composition from the US North Atlantic GEOTRACES transect. *Deep-Sea Res. Part II-Top. Stud. Oceanogr.* **116**, 208–225.
- Page K., Nanson G. and Price D. (1996) Chronology of Murrumbidgee River palaeochannels on the Riverine Plain, southeastern Australia. *J. Quat. Sci.* **11**, 311–326.
- Page K. J., Kemp J. and Nanson G. C. (2009) Late Quaternary evolution of Riverine Plain paleochannels, southeastern Australia. *Aust. J. Earth Sci.* **56**, 19–33.
- Paul M., Bridgestock L., Rehkamper M., van de Flierdt T. and Weiss D. (2015a) High-precision measurements of seawater Pb isotope compositions by double spike thermal ionization mass spectrometry. *Anal. Chim. Acta* **863**, 59–69.
- Paul M., van de Flierdt T., Rehkamper M., Khondoker R., Weiss D., Lohan M. C. and Homoky W. B. (2015b) Tracing the Agulhas leakage with lead isotopes. *Geophys. Res. Lett.* **42**, 8515–8521.
- Petherick L., Bostock H., Cohen T. J., Fitzsimmons K., Tibby J., Fletcher M. S., Moss P., Reeves J., Mooney S., Barrows T., Kemp J., Jansen J., Nanson G. and Dosseto A. (2013) Climatic records over the past 30 ka from temperate Australia – a synthesis from the Oz-INTIMATE workgroup. *Quat. Sci. Rev.* **74**, 58–77.
- Piotrowski A. M., Lee D. C., Christensen J. N., Burton K. W., Halliday A. N., Hein J. R. and Gunther D. (2000) Changes in erosion and ocean circulation recorded in the Hf isotopic compositions of North Atlantic and Indian Ocean ferromanganese crusts. *Earth Planet. Sci. Lett.* **181**, 315–325.
- Piotrowski A. M., Goldstein S. L., Hemming S. R., Fairbanks R. G. and Zylberberg D. R. (2008) Oscillating glacial northern and southern deep water formation from combined neodymium and carbon isotopes. *Earth Planet. Sci. Lett.* **272**, 394–405.
- Piotrowski A. M., Galy A., Nicholl J. A. L., Roberts N., Wilson D. J., Clegg J. A. and Yu J. (2012) Reconstructing deglacial North and South Atlantic deep water sourcing using foraminiferal Nd isotopes. *Earth Planet. Sci. Lett.* **357**, 289–297.

- Rempfer J., Stocker T. F., Joos F., Dutay J. C. and Siddall M. (2011) Modelling Nd-isotopes with a coarse resolution ocean circulation model: sensitivities to model parameters and source/sink distributions. *Geochim. Cosmochim. Acta* **75**, 5927–5950.
- Reuer M. K., Boyle E. A. and Grant B. C. (2003) Lead isotope analysis of marine carbonates and seawater by multiple collector ICP-MS. *Chem. Geol.* **200**, 137–153.
- Roberts N. L., Piotrowski A. M., McManus J. F. and Keigwin L. D. (2010) Synchronous deglacial overturning and water mass source changes. *Science* **327**, 75–78.
- Robinson L. F., Adkins J. F., Frank N., Gagnon A. C., Prouty N. G., Roark E. B. and van de Flierdt T. (2014) The geochemistry of deep-sea coral skeletons: a review of vital effects and applications for palaeoceanography. *Deep Sea Res. Part II* **99**, 184–198.
- Rudge J. F., Reynolds B. C. and Bourdon B. (2009) The double spike toolbox. *Chem. Geol.* **265**, 420–431.
- Schaule B. K. and Patterson C. C. (1981) Lead concentrations in the northeast Pacific: evidence for global anthropogenic perturbations. *Earth Planet. Sci. Lett.* **54**, 97–116.
- Schlitzer, R., 2015. Ocean Data View. odv.awi.de.
- Shen G. T. and Boyle E. A. (1987) Lead in corals: reconstruction of historical industrial fluxes to the surface ocean. *Earth Planet. Sci. Lett.* **82**, 289–304.
- Shen G. T. and Boyle E. A. (1988a) Determination of lead, cadmium and other trace metals in annually-banded corals. *Chem. Geol.* **67**, 47–62.
- Shen G. T. and Boyle E. A. (1988b) Thermocline ventilation of anthropogenic lead in the western North Atlantic. *J. Geophys. Res. Oceans* **93**, 15715–15732.
- Sherrell R. M., Boyle E. A. and Hamelin B. (1992) Isotopic equilibration between dissolved and suspended particulate lead in the Atlantic Ocean: evidence from ^{210}Pb and stable Pb isotopes. *J. Geophys. Res. Oceans* **97**, 11257–11268.
- Siddall M., Khatiwala S., van de Flierdt T., Jones K., Goldstein S. L., Hemming S. and Anderson R. F. (2008) Towards explaining the Nd paradox using reversible scavenging in an ocean general circulation model. *Earth Planet. Sci. Lett.* **274**, 448–461.
- Sokolov S. and Rintoul S. (2000) Circulation and water masses of the southwest Pacific: WOCE Section P11, Papua New Guinea to Tasmania. *J. Mar. Res.* **58**, 223–268.
- Tachikawa K., Jeandel C. and Roy-Barman M. (1999) A new approach to the Nd residence time in the ocean: the role of atmospheric inputs. *Earth Planet. Sci. Lett.* **170**, 433–446.
- Tachikawa K., Piotrowski A. M. and Bayon G. (2014) Neodymium associated with foraminiferal carbonate as a recorder of seawater isotopic signatures. *Quat. Sci. Rev.* **88**, 1–13.
- Taylor R. N., Ishizuka O., Michalik A., Milton J. A. and Croudace I. W. (2015) Evaluating the precision of Pb isotope measurement by mass spectrometry. *J. Anal. Atm. Spectrom.* **30**, 198–213.
- Thiagarajan N., Gerlach D., Roberts M. L., Burke A., McNichol A., Jenkins W. J., Subhas A. V., Thresher R. E. and Adkins J. F. (2013) Movement of deep-sea coral populations on climatic timescales. *Paleoceanography* **28**, 227–236.
- Thiagarajan N., Subhas A. V., Southon J. R., Eiler J. M. and Adkins J. F. (2014) Abrupt pre-Bolling-Allerod warming and circulation changes in the deep ocean. *Nature* **511**, 75–78.
- Thirlwall M. F. (2000) Inter-laboratory and other errors in Pb isotope analyses investigated using a ^{207}Pb - ^{204}Pb double spike. *Chem. Geol.* **163**, 299–322.
- Todd E., Stracke A. and Scherer E. E. (2015) Effects of simple acid leaching of crushed and powdered geological materials on high-precision Pb isotope analyses. *Geochem. Geophys. Geosyst.* **16**, 2276–2302.
- Townsend A. T. and Seen A. J. (2012) Historical lead isotope record of a sediment core from the Derwent River (Tasmania, Australia): a multiple source environment. *Sci. Total Environ.* **424**, 153–161.
- Trinquier A., Bouman C., Schwieters J. and Lloyd N. (2013) $10^{12}\ \Omega$ amplifiers for high precision isotope ratio measurements of small sample sizes, Technical note 30249. Thermo Fisher Scientific, Bremen, Germany.
- Vallelonga P., Gabrielli P., Balliana E., Wegner A., Delmonte B., Turetta C., Burton G., Vanhaecke F., Rosman K. J. R., Hong S., Boutron C. F., Cescon P. and Barbante C. (2010) Lead isotopic compositions in the EPICA Dome C ice core and Southern Hemisphere Potential Source Areas. *Quat. Sci. Rev.* **29**, 247–255.
- van de Flierdt T., Frank M., Lee D. C. and Halliday A. N. (2002) Glacial weathering and the hafnium isotope composition of seawater. *Earth Planet. Sci. Lett.* **198**, 167–175.
- van de Flierdt T., Frank M., Halliday A. N., Hein J. R., Hattendorf B., Gunther D. and Kubik P. W. (2004a) Deep and bottom water export from the Southern Ocean to the Pacific over the past 38 million years. *Paleoceanography* **19**. <http://dx.doi.org/10.1029/2003pa000923>.
- van de Flierdt T., Frank M., Halliday A. N., Hein J. R., Hattendorf B., Gunther D. and Kubik P. W. (2004b) Tracing the history of submarine hydrothermal inputs and the significance of hydrothermal hafnium for the seawater budget - a combined Pb-Hf-Nd isotope approach. *Earth Planet. Sci. Lett.* **222**, 259–273.
- van de Flierdt T., Hemming S. R., Goldstein S. L. and Abouchami W. (2006) Radiogenic isotope fingerprint of Wilkes Land – Adie Coast Bottom Water in the circum-Antarctic Ocean. *Geophys. Res. Lett.* **33**. <http://dx.doi.org/10.1029/2006gl026020>.
- van de Flierdt T., Robinson L. F. and Adkins J. F. (2010) Deep-sea coral aragonite as a recorder for the neodymium isotopic composition of seawater. *Geochim. Cosmochim. Acta* **74**, 6014–6032.
- Vandergoes M. J. and Fitzsimons S. J. (2003) The last glacial-interglacial transition (LGIT) in south Westland, New Zealand: paleoecological insight into mid-latitude Southern Hemisphere climate change. *Quat. Sci. Rev.* **22**, 1461–1476.
- Vlastelic I., Abouchami W., Galer S. J. G. and Hofmann A. W. (2001) Geographic control on Pb isotope distribution and sources in Indian Ocean Fe–Mn deposits. *Geochim. Cosmochim. Acta* **65**, 4303–4319.
- von Blanckenburg F., O’Nions R. K. and Hein J. R. (1996) Distribution and sources of pre-anthropogenic lead isotopes in deep ocean water from Fe–Mn crusts. *Geochim. Cosmochim. Acta* **60**, 4957–4963.
- Weis D., Kieffer B., Maerschalk C., Barling J., de Jong J., Williams G. A., Hanano D., Pretorius W., Mattielli N., Scoates J. S., Goolaerts A., Friedman R. M. and Mahoney J. B. (2006) High-precision isotopic characterization of USGS reference materials by TIMS and MC-ICP-MS. *Geochem. Geophys. Geosyst.* **7**. <http://dx.doi.org/10.1029/2006gc001283>.
- Wilson D. J., Crockett K. C., van de Flierdt T., Robinson L. F. and Adkins J. F. (2014) Dynamic intermediate ocean circulation in the North Atlantic during Heinrich Stadial 1: a radiocarbon and neodymium isotope perspective. *Paleoceanography* **29**, 1072–1093.
- Wilson D. J., Galy A., Piotrowski A. M. and Banakar V. K. (2015a) Quaternary climate modulation of Pb isotopes in the deep Indian Ocean linked to the Himalayan chemical weathering. *Earth Planet. Sci. Lett.* **424**, 256–268.
- Wilson D. J., Piotrowski A. M., Galy A. and Banakar V. K. (2015b) Interhemispheric controls on deep ocean circulation

- and carbon chemistry during the last two glacial cycles. *Paleoceanography* **30**, 621–641.
- Woodhead J. D. and Hergt J. M. (2000) Pb isotope analyses of USGS reference materials. *Geostand. Newsl.* **24**, 33–38.
- Wu J. F., Rember R., Jin M. B., Boyle E. A. and Flegal A. R. (2010) Isotopic evidence for the source of lead in the North Pacific abyssal water. *Geochim. Cosmochim. Acta* **74**, 4629–4638.
- Zweng, M.M., Reagan, J.R., Antonov, J.I., Locarnini, R.A., Mishonov, A.V., Boyer, T.P., Garcia, H.E., Baranova, O.K., Johnson, D.R., Seidov, D., Biddle, M.M., 2013. World Ocean Atlas 2013, Volume 2: Salinity. In NOAA Atlas NESDIS 74 (ed., Levitus, S.).

Associate editor: Claudine Stirling